Petrosal and bony labyrinth morphology of the stem paenungulate mammal (Paenungulatomorpha) Ocepeia daouiensis from the Paleocene of Morocco

Emmanuel Gheerbrant, Arnaud Schmitt, Guillaume Billet

Petrosal and bony labyrinth morphology of the stem paenungulate mammal (Paenungulatomorpha) *Ocepeia daouiensis* from the Paleocene of Morocco

Emmanuel Gheerbrant[1*], Arnaud Schmitt[1], and Guillaume Billet[1]

[1] *CR2P, Centre de Recherche en Paléontologie, Paris, UMR 7207 (CNRS, MNHN, UPMC, Sorbonne Universités), Paris, France*

**corresponding author: emmanuel.gheerbrant@mnhn.fr*

Abstract

Based on high-resolution computed tomography, we describe in detail the petrosal and inner ear anatomy of one of the few known African stem paenungulates (Paenungulatomorpha), *Ocepeia daouiensis* from the Selandian of the Ouled Abdoun phosphate basin (Morocco). The petrosal of *Ocepeia* displays some remarkable, probably derived features (among eutherians) such as relatively small pars cochlearis, pars canalicularis, and labyrinth (incl. small semicircular canals), a large wing-like pars mastoidea, a large and inflated tegmen tympani, and the dorsoventral orientation of the large canal for the ramus superior. The presence of small semicircular canals in *Ocepeia* is an interesting shared trait with tenrecoidean afrotherians. Otherwise, and consistent with a general primitive skull morphology, the middle ear and labyrinth of *Ocepeia daouiensis* is characterized by many plesiomorphic traits close to the eutherian generalized plan. This adds to the rather generalized morphology of the earliest crown paenungulates such as *Eritherium*, *Phosphatherium*, and *Seggeurius* to support an ancestral paenungulatomorph morphotype poorly derived from the eutherian pattern. As a result, *Ocepeia* provides key morphological and fossil data to test phylogenetic relationships of the Afrotheria (including Paenungulatomorpha) at the placental root mostly inferred from molecular studies.

Key words: skull; petrosal; bony labyrinth; cochlea; computed tomography (CT); Paleocene; Africa; Ocepeia; Paenungulata; Afotheria.

Introduction

The condylarth-like mammal *Ocepeia daouiensis* from the Paleocene-Selandian (Yans et al. 2014; Kocsis et al. 2014) of the Ouled Abdoun Basin, Morocco, is the best known of the earliest African placentals (Gheerbrant, 2010; Gheerbrant et al. 2014). Recently described material includes the well-preserved skull MNHN.F.PM45. Its study by Gheerbrant et al. (2014) supported that *Ocepeia daouiensis* is related to the Paenungulata as a stem taxon (Paenungulatomorpha; see Fig. 1). The paenungulate stem relationship of *Ocepeia* was also found in recent works of Gheerbrant et al. (2016, 2018) and Zack et al. (2019). *Ocepeia* is actually the only known stem paenungulate together with *Abdounodus hamdii* (Gheerbrant et al. 2016).

The skull MNHN.F.PM45 preserves in particular the braincase and labyrinth endocasts. In this work we describe and study in detail the petrosal morphology and the bony inner ear morphology of *Ocepeia daouiensis* that was reconstructed as a 3D endocast model from a micro CT scan of the skull MNHN.F.PM45. The reconstruction and study of the inner ear of *Ocepeia daouiensis* were made based on both left and right petrosals preserved in specimen MNHN.F.PM45 (Gheerbrant et al. 2014). The right and left semicircular canals are perfectly aligned in profile in lateral view, showing that the petrosals are not distorted in MNHN.F.PM45.

The anatomy of the petrosal and inner ear of the afrotherians and its phylogenetic significance were only recently investigated, and mostly based on the study of extant taxa (Ekdale, 2013). However, several recent important fossil discoveries in the Paleogene of Africa provided new key data on early afrotherians, including proboscideans (Schmitt & Gheerbrant, 2016), embrithopods (Benoit et al. 2013c), hyracoids (Benoit et al. 2015a) and macroscelideans (Benoit et al. 2013b). *Ocepeia* adds to these fossil discoveries and provides the first direct evidence on the ancestral petrosal and labyrinthine morphology of the Paenungulata.

Material and Methods

Collections, institutional abbreviations

OCP DEK/GE: Collections of the Office Chérifien des Phosphates, Khouribga, Morocco
MNHN.F: fossil collection of the Museum National d'Histoire Naturelle, France.
STIPB: Steinmann Institut Paläontologie Bonn.

Scan, modelisation, softwares

MNHN.F.PM45 was investigated by high-resolution computed tomography (µCT) at the AST – RX platform of the MNHN, Paris, using a GE Sensing and Inspection Technologies phoenix|x-ray v|tome|x L240-180 CT scanner. We used the microfocus RX source 240kV/320W, detector 400 × 400 mm with a matrix of 2024 pixels (pixel size: 200x 200µm). Scan parameters:

Voltage=95 kV; Current=265 µA; Isotropic voxel size of 0.02550441 mm. Data were reconstructed using datos|x reconstruction software (Phoenix|x-ray, release 2.0) and then exported into 16 bits TIFF images. We used the softwares MIMICS (® Materialise 2007, Release 11.1) and Avizo 7.1.1 (Visualization Science Group) for the analysis, 3D modelisation, visualisation and measurement of the tomographies. The 3D models of the petrosals and bony labyrinths will be deposited and freely accessible on the Morphomuseum repository at https://morphomuseum.com/.

Measurements (Fig. 2)

The volume of the petrosal was measured directly on the 3D model with MIMICS. Volumes of the labyrinth were obtained using both the softwares MIMICS and Ariadne (David et al. 2016) that computes volumes, lengths, areas and angles (see below). The main goal of the Ariadne software is to infer functional capacities of fossil taxa based on measurements of their bony labyrinth, and through comparisons with the membranous ducts of relatively close taxa. In addition, the Ariadne software can be used to simply provide several bony measurements (i.e. semicircular central streamline length, cochlear length) that may be useful for further comparisons and which are presented for *Ocepeia* in this paper. The cochlear volume was obtained by separating the cochlear part from the vestibular part using GEOMAGICS Studio Studio 2012. The superior extremity of the cochlear canal as well as the fenestra vestibuli were included in the cochlear part. On the other hand, the saccule was included in the vestibule part.

We measured with the software MIMICS the inner ear height (IEH) following Billet et al. (2015) as the linear distance between the dorsal apex of the crus commune and the ventral apex of the cochlea. The petrosal size index of *Ocepeia* was measured following Billet et al. (2015) as the mean of the longest linear dimensions of the petrosal (excluding the mastoid part): the medial length and anterior width of the tympanic face (PET L and PET W), and the cerebellar height (PET H).

The **stapedial ratio** (Fig. 2A) was calculated following Segall (1970: L/W with L = length and w = width of the fenestra vestibuli). Calculation of the cochlear curvature follows West (1985). The number of turns of the cochlea is measured following the protocol of West (1985). The **aspect ratio** of the cochlea (Fig. 2B) was calculated according to the formula found in Ekdale & Rowe (2011): H/W with H= height and W= width of the cochlea. Other linear measurements of the labyrinth were obtained using the same custom software used for the labyrinth volumes. The length of the cochlea was obtained through the sum of the distance of consecutive landmarks and semilandmarks placed along the cochlea using AVIZO 7.1.1 (Fig. 2C-D) and calculated with the Ariadne software. The first anatomical landmark was located at the point of the external portion of the cochlea located in the continuation of the major axis of the fenestra vestibuli. The semilandmarks were then placed manually at approximately regular distance along the external portion of the cochlea (which follows the basilar membrane) (n~50). The last anatomical landmark was placed at the tip of the helicotrema. For both the cochlea and semicircular canals (see below), there was no sliding procedure for the semilandmarks as these were only used in order to mark curves for non-linear measurements (e.g., cochlea length, semicircular canal length).

Measurements of the semicircular canals were also landmark-based, but using central streamlines of the canals calculated with the AutoSkeleton feature of AVIZO 7.1.1 (following Gunz et al. 2012). The central streamline is the line that follows the center of the bony canal over its full length. It is obtained via the Autoskeleton functionality of the software Avizo. The internal landmarks of the semicircular canals (lighter grey landmarks that are also represented without the isosurface in Fig. 2C, D, E) are placed on this streamline. The central streamline length of a semicircular canal is the sum of the distances between these landmarks (central streamline landmarks) and the ampullar landmarks (the two very light grey landmarks on each

canal, Fig. 2). The crus commune length consists of the sum of the distances between consecutive internal landmarks, and the semilandmarks were placed manually at approximately regular distance along the central streamline of the crus commune (from the intersection of the anterior and posterior canals streamline to the basis of the crus commune). The average section radius of the crus commune was given directly by the Ariadne software. It corresponds to the mean of the crus commune radii taken at different sections of the crus commune. We used these two values to calculate the **average thickness ratio** (average section radius / crus commune length * 100). This ratio gives a quantitative value that expresses the global thickness of the crus commune. Crus commune with a high ratio tend to be thicker and stockier than crus commune with a low ratio.

The semicircular canal length was calculated as the sum of the distances between consecutive landmarks and semilandmarks of the slender canal. For the anterior and posterior canals, the measurement starts at the center of the ampulla (at the level of the crista ampullaris) and ends at the level of the intersection of the two canals (first internal landmark of the crus commune). For the lateral canal, the measurement starts at the center of the ampulla and ends at the intersection with the lateral utricle. The average section radius was calculated in the same manner as for the crus commune average section radius. It expresses the mean section radius of the slender part of the canal. The average **thickness ratio** of each semicircular canal was calculated as the following formula: (average section radius / semicircular canal length) x 100. The mean of these three ratios expresses the **global thickness** of the semicircular canals quantitatively.

The angles between the semicircular canals were also given directly by the Ariadne software. Measuring manually these angles can be tricky because the semicircular canals are rarely perfectly planar. The software uses the landmarks to determine the functional plane of each semicircular canal (David et al. 2016). The angles were then compared between the functional planes of the canals.

Calculation of the **radii of curvature** of the semicircular canals uses the Spoor–Zonneveld equation (Spoor & Zonneveld, 1998): R= ((L+W)/2) x 0.5, with L = length and W = width of the canals. Height and width of the semicircular canals were calculated from the center of the canal to the vestibule (which includes the ampullas) and following protocol of Macrini et al. (2010).

Figure 2 summarizes our measurement protocol of the bony labyrinth of *Ocepeia daouiensis*.

Comparisons

Anatomical comparisons were made with most early eutherians and placentals in which the petrosal and labyrinth are described based on the available CT observations: *Kulbeckia* (Ekdale, 2013), zhelestids (Ekdale & Rowe, 2011; Ekdale, 2013), *Zalambdalestes* (Ekdale & Rowe, 2011), *Protungulatum* (Orliac & O'Leary, 2016), *Carsioptychus* (Cameron et al. 2019), *Chriacus* (Bertrand et al. 2019), *Hyopsodus* (Ravel & Orliac, 2015), *Diacodexis* (Orliac et al. 2012), *Alcidedorbignya* (Muizon et al. 2015), *Leptictis* and *Leptictidium* (Ruf et al. 2016), *Notostylops* (Macrini et al. 2010, 2013), early diverging litopterns and notoungulates (Billet & Muizon, 2013; Billet et al. 2015), *Arsinoitherium* (Benoit et al. 2013c), *Prorastomus* (Benoit et al. 2013a), the undetermined sirenian from Chambi (Benoit et al. 2013a), *Chambius* (Benoit et al. 2013d), *Seggeurius* (Benoit et al. 2015a), *Eritherium* (Schmitt & Gheerbrant, 2016), *Phosphatherium* (Schmitt & Gheerbrant, 2016), *Numidotherium* (Benoit et al. 2013c; Court, 1992). Comparative anatomical data for extant placentals and especially afrotherians come from Benoit et al. (2015b) and Ekdale (2013). We used an anatomical terminology that generally follows the English equivalents of terms from the Nomina Anatomica Veterinaria, 5th edition (Waibl et al. 2005). When this practice was not appropriate (see Wible, 2010), terms were taken from the general comparative literature cited above.

Abbreviations

ASC: anterior semicircular canal, LSC: lateral semicircular canal, PSC: posterior semicircular canal, SC: semicircular canal.

The petrosal of *Ocepeia* (Figs 4-5)

The basicranium of *Ocepeia daouiensis* preserves both right and left petrosals (see Gheerbrant et al. 2014). While the petrosal is damaged in the mastoid region, the part containing the inner ear is well preserved. Since there are no significant differences between the left and the right ears, the measurements given below are an average of the left and right ear measurements, except when mentioned otherwise.

The overall position and extension of the petrosal, as well as its general morphology within the skull, are displayed in figure 3**.** Figures 4-5 provide detailed views of the petrosal**.** The petrosal index size measured following Billet et al. (2015) is 8.44 mm. The main features of the middle ear were previously described by Gheerbrant et al. (2014) - only new observed anatomical characters are described and compared below.

With respect to Gheerbrant et al. (2014), the comparisons are further developed with early paenungulates such as the hyracoid *Seggeurius amourensis*, the proboscideans *Eritherium azzouzorum* and *Phosphatherium escuillei*, and also the unnamed sirenian from Chambi (Benoit et al. 2013a). *Ocepeia* shares a noticeable general resemblance with early paenungulates such as *Seggeurius, Eritherium* and the unnamed sirenian from Chambi. It includes the shape and robust construction of the *pars cochlearis* (Benoit et al. 2015a) and the inflated and barrel-like *tegmen tympani*, although the latter is slightly more inflated in *Eritherium*. In rostro-ventral view, the morphology of the petrosal of *Ocepeia* and *Eritherium* is strikingly similar. Both taxa share in particular a large foramen in the *tegmen tympani* probably for the ramus superior of the stapedial artery (Fig. 4). It suggests the presence of the stapedial artery in *Ocepeia,* as in *Seggeurius*. In *Ocepeia*, the canal for the ramus superior is characterized by an original orientation from its ventral opening within the *tegmen tympani*: it runs dorsally, and slightly laterally (Fig. 5B). In

190 *Eritherium*, it runs more anteriorly. *Ocepeia* is very similar to *Eritherium* in the morphology of
191 the stylomastoid notch that is delimited anterolaterally by a large bony ridge, the tympanohyal
192 (Fig. 4). This morphology, also seen in *Phosphatherium* (Gheerbrant et al. 2005, fig. 7), is likely
193 plesiomorphic for paenungulates. The promontorium is characterized by a very anterior position
194 in the petrosal, in association with a long and large mastoid apophysis in *Ocepeia* (Fig. 3A). The
195 promontorium shows a thick rostral tympanic process and a concave medial border representing
196 the sulcus of the inferior petrosal sinus (ips, Fig. 4). This sulcus is also well developed in
197 *Eritherium*. Medial to the sulcus of the inferior petrosal sinus, there is a flattened medial edge
198 that is reminiscent of a medial flange. The fenestra vestibuli of *Ocepeia* is elliptical. As in
199 *Eritherium,* the cochlear canaliculus (*aquaeductus cochleae*) opens ventro-medially in the
200 jugular fossa, more dorsally and more medially than the external aperture of the cochlear fossula
201 (which leads to the fenestra cochleae; see Wible et al. 2009, Billet and Muizon, 2013) (Fig. 4C).
202 The secondary facial foramen is visible on the right petrosal. It opens just laterally to the canal
203 for the ramus superior, well anterior to the fenestra vestibuli (Fig. 4B). It covers the cavum
204 supracochleare ventrally whose channel is directed somewhat more oblique than its posterior
205 prolongation, the facial sulcus. Anteriorly, the hiatus Fallopii is present as a small opening on the
206 anterior edge of the petrosal (Fig. 4A-B). Posterior to it, a large depressed area seems to be
207 present on the anterolateral portion of the promontorium, which could then correspond to the
208 tensor tympani fossa. However, this region has experienced some crushing and caution is thus
209 required for this identification. Posterior to the secondary facial foramen, the facial sulcus
210 borders the tympanic surface of the promontorium laterally. The facial sulcus is bordered
211 laterally by a low crista parotica (possibly damaged). The exact outline of the epitympanic recess
212 is unclear but it lies on the lateral aspect of the petrosal, dorsolaterally to the crista parotica and
213 posterior to the tegmen tympani. In its posterior part, the fossa incudis forms an oval-shaped
214 depression (Figs. 4B & 5A). There is no clear distinction of the stapedial fossa from the facial

sulcus posteriorly, showing that the former is not very well marked, except for a distinct widening of the sulcus (Fig. 4C). In *Eritherium*, the stapedial fossa is not only wider but deeper and thus more distinct from the facial sulcus. Ventromedial to the stapedial fossa, the external aperture of the cochlear fossula is bordered posteriorly by a much reduced postpromontorial tympanic sinus in *Ocepeia* (very thin anteroposteriorly and stretched mediolaterally). This space is bordered posteriorly by a large and anteroposteriorly thick medial caudal tympanic process that faces the entire external aperture of the cochlear fossula posteriorly (Fig. 4B). This appears to be different from *Eritherium* in which the external aperture of the cochlear fossula is not bordered by a postpromontorial sinus nor by a medial caudal tympanic process (*contra* Schmitt & Gheerbrant, 2016), but is just opening directly ventromedially to the stapedial fossa. This thick medial caudal tympanic process is present in *Seggeurius* where it is called "swelling on the septum metacochleare" by Benoit et al. (2015a). A notch is present on the medial aspect of the postpromontorial tympanic sinus of *Ocepeia*, between the medial caudal tympanic process and the medial buttress of the external aperture of the cochlear fossula, possibly for the passage of the tympanic nerve or for the auricular branch of the vagus nerve (see MacPhee, 1981; Evans & de Lahunta, 2012; Billet et al. 2015; Muizon et al. 2015). In cerebellar view (Fig. 5C), the fossa subarcuata of *Ocepeia* is deep as in *Eritherium*. However, the shape of the fossa differs between the two taxa: in *Ocepeia*, the fossa has the shape of a lightly flattened cone while it is almost spherical in *Eritherium*. The fossa subarcuata is much deeper in *Ocepeia* and *Eritherium* than in *Phosphatherium*, and a little deeper than in *Seggeurius*. The internal auditory meatus and the fossa subarcuata of *Ocepeia* are comparable in size, as in *Eritherium*. In *Seggeurius* and *Phosphatherium* the area of the fossa subarcuata is by contrast larger than the internal auditory meatus. The *foramen acusticum superius* and *inferius* of *Ocepeia* are separated by a distinct and short *crista transversa*. It is as thick and short as in *Eritherium,* and thicker than in

239 *Phosphatherium* which displays a very narrow and long crista. The *crista transversa* is not
240 distinct in the cerebellar views of the petrosal of *Seggeurius* figured in Benoit et al. (2015).

241 On the dorsolateral (or squamosal) surface of the petrosal, a large sulcus is present in
242 continuation with the canal for the ramus superior of the stapedial artery. This sulcus runs in
243 posterodorsal direction on the dorsolateral edge of the petrosal (labelled stb? on Fig. 5D). On the
244 right petrosal, another sulcus seems to be present, and also runs towards the posterior direction,
245 dorsal to the base of the tegmen tympani (labelled pts? on Fig. 5A, D). This sulcus is not clearly
246 marked on the left petrosal, but the skull MNHN.F.PM45 is damaged in its left side, including
247 the left petrosal (whereas the right side and right petrosal are better preserved). The sulcus
248 running on the dorsolateral edge of the petrosal (stb? on Fig. 5D) likely represents a sulcus for a
249 posterior temporal ramus as it seems to connect with the large posterior temporal foramen in
250 *Ocepeia* (Gheerbrant et al. 2014: fig. 2). It may also have housed the capsuloparietal emissary
251 vein on its posterior portion (see Billet et al. 2015). The sulcus running directly dorsal to the
252 tegmen tympani (labelled "pts?" in Fig. 5) probably represents the posttemporal sulcus for the
253 diploëtica magna vessels (it could not be firmly confirmed from observations of the virtual slices
254 through the skull as the area that would correspond to the posttemporal canal is damaged,
255 especially posteriorly).

256 In *Eritherium*, a sulcus similar to those described in *Ocepeia* and running dorsally and then
257 posterodorsally on the dorsolateral edge of the squamosal surface of the petrosal is present, and
258 was recognized as a prootic sinus (Schmitt & Gheerbrant, 2016). The prootic canal is generally
259 absent in placentals, except in the extant *Solenodon* (Wible, 2008). Here the course of this sulcus
260 in *Eritherium* corresponds much better with the posttemporal canal and/or a sulcus for temporal
261 rami (Wible, 1993; Billet et al. 2015; Muizon et al. 2015), as found in *Ocepeia*. In addition, the
262 presence of a sulcus of the sigmoid sinus dorsomedial to the aforementioned sulcus (Schmitt &

Gheerbrant, 2016: fig. 2C) is erroneous in *Eritherium* and corresponds to a broken area partly filled with cancellous bone.

The pars mastoidea is remarkably expanded, it is longer than the pars cochlearis and it reaches the occipital face (Figs. 3, 5-6). The pars mastoidea forms a mediolaterally compressed wing-like bony blade that is elongated and oblique anteroventral to posterodorsal (Fig. 3). The posterior extent of the pars mastoidea is hard to determine accurately as the bony sutures in the posteriormost part of the skull with the exoccipitals, parietal and squamosal are indistinct in a damaged area of the skull. There is likely a small sliver of bone of the pars mastoidea posteriorly exposed between the parietal and exoccipital (Fig. 3), that would thus participate to the external occipital face (mastoid exposure condition), but its extent is not determinable. The pars mastoidea of *Ocepeia daouiensis* is substantially pneumatized with numerous and large trabeculae, especially in its dorsal part toward the supraoccipital which is itself also highly pneumatized (Gheerbrant et al. 2014).

In conclusion, among paenungulates the petrosal of *Ocepeia* is more similar to that of *Eritherium*. Resemblances are seen in the general proportions, and in several detailed features (a deep fossa subarcuata which size is comparable to that of the internal auditory meatus, a very inflated barrel-like *tegmen tympani*, a short crista transversa, the presence of a large foramen for the ramus superior of the stapedial artery). As a whole, the middle ear of *Ocepeia* shows a combination of (1) plesiomorphic eutherians traits such as the deep fossa subarcuata, the promontorium weakly inflated and flanked by a flattened medial edge (associated to a thick rostral tympanic process of uncertain evolutionary polarity), and a postero-medial external aperture of the cochlear fossula (see Discussion), and (2) paenungulate features such as an inflated and large tegmen tympani. The pierced tegmen tympani (foramen for the ramus superior of the stapedial artery), known in several other eutherian groups, is also probably plesiomorphic amongst placentals (Wible et al. 2001; Billet and Muizon, 2013; Muizon et al. 2015).

The inner ear bony labyrinth

Dimensions of the inner ear bony labyrinth

The total volume of the inner ear bony endocast of *Ocepeia daouiensis* is 17.53 mm^3 and its inner ear height (IEH; Billet et al. 2013) is 5.69 mm (Table 1). By comparison to the skull length and body size of *O. daouiensis* (SL~ 90 mm, estimated body mass 3.5 kg; Gheerbrant et al. 2014), this is a relatively small inner ear. Among afrotherians, *Procavia* has a relative labyrinth volume to body mass and skull length noticeably greater than *Ocepeia* (*Procavia* specimen STIPB-M6605: lab. vol.= 33.84 mm^3, SL= 76 mm, BM= 3800 g.; BM in Nowak, 1999). Comparison of the semicircular canals size (radius of curvature, SCR) relative to the body mass following the method of Spoor et al. (2007) (see Fig. 8) also indicates that *Procavia* (taken from Benoit et al. 2015; see also similar values in Ekdale, 2013) has a larger inner ear, which is confirmed by its higher IEH (IEH of specimen STIPB-M6605 = 8.16 mm, i.e. 143% of *Ocepeia*). We extended the sample of the placental species studied by Spoor et al. (2007) with the addition of several afrotherians for our comparison of the proportions of the labyrinth in *Ocepeia*. It shows that *Ocepeia* shares a relative small size of the semicircular canals with several tenrecoid afrotherians such as *Potamogale*, *Tenrec*, *Hemicentetes* and *Chrysochloris* (Fig. 8). By contrast other afrotherians such as *Procavia* (hyracoid), *Orycteropus* (tubulidentate), *Macroscelides* and *Rhynchocyon* (macroscelidids) have larger semicircular canals relative to their body mass.

The 3D reconstructed digital models display a relative small size of the inner ear of *Ocepeia daouiensis* within the skull (Fig. 3). It also displays a relative small size of the bony labyrinth within the petrosal (Figs. 3 and 6). This is well distinctive from the small-sized *Protungulatum* where the bony labyrinth seems to occupy a large portion of the internal volume of the petrosal (Orliac & O'Leary, 2016). In comparison, the relative small size of the inner ear of *Ocepeia daouiensis* within the petrosal seems to be related to both its large and inflated tegmen tympani and its very large wing-like mastoid portion. The ratio of the petrosal index size (PET size) to the

inner ear height (IEH) of *Ocepeia* (Table 1) indicates that the relative labyrinth and petrosal size does not depart from the general proportions and growth trend seen in other measured placental mammals (Billet et al. 2015). This is also true for *Eritherium* and *Phosphatherium* (Fig. 8 and SI2). This suggests that this is actually the petrosal (pars cochlearis and pars canalicularis), and not only the labyrinth, that is small relative to the BM and skull length in *Ocepeia.* In this regard, it is worth noting that the petrosal index size is based on linear measurements that do not include the pars mastoidea which is large in *Ocepeia* especially relative to the pars cochlearis (Gheerbrant et al. 2014: p. 7).

Cochlea (Figs. 6 - 7)

Description and comparisons

The cochlea of *Ocepeia daouiensis* is large with respect to the vestibule size. The volume ratio of the cochlea with respect to the whole labyrinth is 66 %. This is similar to zhelestids (Ekdale & Rowe, 2011; Orliac & O'Leary, 2016), and this is greater than in the reconstructed ancestral morphotype of placentals and of afrotherians (Ekdale, 2013). The relative great proportion of the cochlea in *Ocepeia* might be an eutherian plesiomorphic condition (Ekdale, 2013). The cochlea length is 19.2 mm. By comparison, it is 16.05 mm in *Leptictidium* (Ruf et al. 2016) which has a slightly larger IEH (6.44 mm) and a much smaller body size (BM: 466-627 g.). In the same way, the *Leptictis* species studied by Ruf et al. (2016) has a close cochlear length (18.02 mm) and IEH (5.3 mm), for a much smaller body size (BM: 400-1000 g) than *Ocepeia*. As noted above, it confirms the small size of the bony labyrinth and petrosal (pars cochlearis and pars canalicularis) in *Ocepeia daouiensis.*

The number of coils of the cochlea measured following the method of West (1985) is 2.13 (765°). A cochlea with at least two turns is generally representative of the placental derived condition by contrast to most Cretaceous eutherians that have only 1-1.5 turns (Meng & Fox, 1995; Ekdale & Rowe, 2011). However, some early diverging crown paenungulates such as

Numidotherium (540°-576°), *Prorastomus* (550°) and *Seggeurius* (688°), and also some Paleocene placentals such as *Protungulatum* (553°), *Carsioptychus* (600°) and the pantodont *Alcidedorbignya* (540°) have a less coiled cochlea, with less than two turns.

The ratio of the radius of the spiral base and spiral apex, also called grade of curvature of the cochlea, is low: R_{base}/R_{apex}= 2.75. The spiral plane (lower coil) is oblique antero-dorsally, with an angle of about 50-60° with respect to the plane of the LSC, depending of the angle of view. This is significantly greater than in Cretaceous eutherian mammals; in zhelestids for instance, the plane of the basal coil is tilted at 34° with respect to LSC plane (Ekdale & Rowe, 2011). The pantodont *Alcidedorbignya* also has a smaller angle of the basal cochlear coil to LSC plane (35-21°). The coiling is subplanar, as in the primitive eutherian condition: the basal coil is more or less below the upper coil but the spiral coils do not separate fully from each other along the coiling axis (Fig. 7C). The height to width aspect ratio of the cochlea cast is 0.72, close to the values of *Carsioptychus*, *Hyopsodus* and the afrotherians *Moeritherium,* the undetermined sirenian from Chambi and *Chambius*. In the coiling plan, the spiral coils are well separated from each other (Fig. 7B) as in the zhelestids, *Carsioptychus, Hyopsodus* and *Alcidedorbignya*. This character is uncommon amongst placentals. The spiral coils are in particular in contact (i.e. coalescing) in basal paenungulates such as *Eritherium*, *Numidotherium, Prorastomus*, the undetermined sirenian from Chambi (Benoit et al. 2013a), *Seggeurius* and *Arsinoitherium*. The basal coil is enlarged in the area of the fenestra cochleae. The apical coil has a section diameter comparable to the basal coil, and the helicotrema is large, but not inflated. This is distinctive from *Notostylops*, but of uncertain polarity among eutherians. In ventral view there is a quite distinct apical lacuna for the bony modiolus at the spiral apex.

The secondary bony spiral lamina extends on nearly all the basal coil (340-360° from f. vestibuli; i.e. about 46% of cochlear can. length). This is comparable to some Cretaceous eutherians such as zhelestids and zalambdalestids (Ekdale & Rowe, 2011), and to *Protungulatum*

and *Eritherium*. The secondary bony spiral lamina is a little shorter along the cochlear canal in *Phosphatherium*, and more so in other crown placentals such as *Notostylops*, *Hyopsodus* and *Diacodexis*. The width of the secondary bony spiral lamina within the cochlear canal is very small (width from lateral wall of cochlear canal of about 0.1 mm). The secondary bony spiral lamina is located high (dorsal) on the cochlear canal, indicating asymmetric development of the scalae. The horizontal (XZ 740-760) and transverse (coronal) sections (XY 489) show indeed that the scala vestibuli was larger than the scala tympani (see Gheerbrant et al. 2014, fig. 7). The primary spiral bony lamina is well developed (width from axial wall of modiolus estimated as 0.3 mm); the distance from the primary basal spiral lamina to the lateral wall of the cochlea (vestibular fissure), corresponding to the width of the basilar membrane (laminar gap), is about 0.3 mm (approximately same at base and apex). The modiolus appears in our CT scan sections of the petrosal as a darker area indicating bone of typically lower density. The ganglion canals (spiral canal) are poorly visible, but they seem distinct on some sections of the left petrosal (e.g., sections XZ 753, XY 491).

The fenestra vestibuli opens well below the lateral ampulla. It opens perpendicular with respect to the external aperture of the cochlear fossula, as in *Seggeurius* (Benoit et al. 2015). It is elliptical with a high stapedial ratio of 2.05. A high stapedial ratio value is also found in *Protungulatum* (2.1) and Cretaceous eutherians such as *Kulbeckia* (2.0). The stapedial ratio is lower in most paenungulates, even in the primitive genera such as *Eritherium* (1.57), *Phosphatherium* (1.62), *Numidotherium* (1.8) and *Seggeurius* (1.79). A high stapedial ratio might correspond to the primitive placental and eutherian condition (Segall, 1970; Macrini et al. 2010), but there is some variation amongst placentals (Ruf et al. 2016). For instance, a high value of stapedial ratio is seen in some paenungulates such as the indeterminate sirenian from Chambi (1.95) and the extant genera *Dendrohyrax* (2.5; Benoit et al. 2015) and *Procavia* (2.1). Although smaller than the external aperture of the cochlear fossula, the fenestra vestibuli is

rather large, especially relative to paenungulates such as proboscideans (Table 1). This is the generalized condition and this is distinctive from *Phosphatherium* and *Numidotherium* (Schmitt & Gheerbrant, 2016). The external aperture of the cochlear fossula is large and postero-medially located with respect to the f. vestibuli. Its outline is noticeably elongated dorso-ventrally.

The cochlear canaliculus (perilymphatic duct) is well separated (distant) from the external aperture of the cochlear fossula, with an opening on the dorsal face of the cochlea. It is long and extends postero-dorso-medially. A posterior orientation of this canal is also observed in the zhelestids and in *Protungulatum*. The canal is large in diameter with respect to many placentals (e.g., *Notostylops*, *Protungulatum*), but similar to some marsupials (Schmelzle et al. 2007). Its cross-section is larger than that of the semicircular canals, and its opening enlarges nearly as the size of the external aperture of the cochlear fossula.

The aqueductus vestibuli (endolymphatic canal) is quite distinct. It originates from the vestibule just medial and anterior to the crus commune, as in zhelestids, *Alcidedorbignya* and *Protungulatum*. From the vestibule, it extends postero-dorsally, parallel to the crus commune to which it is closely appressed. Its base is bulged as in *Protungulatum*. It is very thin on most of its length, with a diameter much smaller than that of the semicircular canals.

Table 1: Measurements of the cochlea and fenestrae of the bony labyrinth of *Ocepeia daouiensis* (mm)

Cochlea of *Ocepeia daouiensis*	
Volume of the labyrinth	17.5 mm^3
Volume of cochlea	11.65 mm^3
IEH Inner Ear Height	5.69 mm
PET size	8.44 mm
Number of coils	2.13 (765°)
Relative volume of the cochlea	66%
Length of cochlear canal	19.2 mm
Stapedial ratio	2.05
Ext. apert. coc. fossul. area	0.312 mm^3
Aspect ratio	0.72
Max Width of cochlea (diameter)	3.55 mm
Max Height of cochlea	2.1 mm

Functional anatomy of the cochlea of Ocepeia daouiensis*: Estimation of the frequency range of hearing*

The cochlear size was shown to be related to the hearing sensitivity in mammals (e.g., West, 1985; Kirk & Gosselin-Ildari, 2009). We followed the predictive equations of West (1985) and Meng & Fox (1995) to estimate the frequency range of the hearing in extant and fossil mammals based on the dimensions of the cochlea. Our calculations based on these equations indicate that the range of audible frequencies of *Ocepeia daouiensis* is between **29.5 and 0.12 kHz** at 60dB sound pressure level (number of cochlear coils: 2.125; length of cochlea: 19.2 mm; see Table 2). By comparison to the values recorded by Meng & Fox (1995: Fig. 6), *Ocepeia daouiensis* is characterized by an intermediate sensitivity for low frequency sounds, between the lower limit of extant placental mammals and the higher limit of Cretaceous therian mammals studied by Meng & Fox (1995, Fig. 6). The low-frequency hearing limit of *Ocepeia* is also significantly lower than that in *Protungulatum* (1.21 kHz in Orliac & O'Leary, 2016). *Ocepeia* consistently has a longer basilar membrane (cochlear canal length) than in Cretaceous eutherians and *Protungulatum*. In addition, the weak development in width of the secondary bony lamina in *Ocepeia* agrees with a relative sensitivity for low frequency sounds. The low-frequency hearing limit of *Ocepeia* calculated following Manoussaki et al. (2008) is 0.548 kHz (at 60 dB) which is higher than value calculated following West (1985) and Meng & Fox (1995) and close to *Diacodexis* (Orliac & O'Leary 2012). However, the reliability of the procedure of Manoussaki et al. (2008) was questioned (e.g. Orliac & O'Leary 2016). *Ocepeia* also has lower value of the upper-frequency limit with respect to those of the Cretaceous therians studied by Meng & Fox (1995, Fig. 6).

We calculated the same hearing frequency range of *Ocepeia* using other published equations by Rosowski & Graybeal (1991) and Rosowski (1992) based on basilar membranous length (= length of cochlear canal): see Table 2. The resulting hearing range of *Ocepeia* at 60 dB was between 31.73 and 0.37 kHz. This is similar to the results calculated from West (1985) method for the high-frequency limit, but higher for the low-frequency limit (at 60 dB SPL). It should be however noted that the relevance of the prediction models of high frequency hearing in mammals such as those of Rosowski (1992) have been recently questioned (e.g., Harper & Rougier 2018).

The upper high frequency limit of *Ocepeia* was also estimated based on the interaural distance (Hefner & Hefner, 2008; Ravel & Orliac, 2015). It provides a value (Table 2) in the range of ultrasounds sensitivity (sound frequencies > 20 kHz, e.g. Ravel & Orliac, 2015),

448 although the restriction of the secondary bony lamina to the cochlea first turn indicates that
449 *Ocepeia* obviously was not specialised for high frequency hearing.
450
451 **Table 2:** Estimation of the hearing frequency range of *Ocepeia* based on its labyrinth
452 dimensions. LF: Low-frequency limit; HF: High-frequency limit. 1. Equation of West (1985),
453 Meng & Fox (1995), based on basilar membranous length (BML=cochlear canal length) and
454 number of coiling (N); Frequency limits at 60 dB Sound Pressure Level: log(LF) = 1.76-1.66
455 log(BMLxN); log(HF) = 2.42-0.994 log(BML/N). 2. Equation of Rosowski and Graybeal (1991)
456 and Rosowski (1992), based on basilar membraneous length (BML); frequency limits at 60 dB
457 Sound Pressure Level: log(LF)=13($BML^{-1.2}$); log(HF) = 391 ($BML^{-0.85}$). 3. Equation of Hefner
458 & Hefner (2008): log of high-frequency limit = –0.4381 x log (functional interaural delay) +
459 2.7137); with functional interaural delay (microseconds)= interaural distance/0.3434 (see also
460 Ravel & Orliac 2015). 4. Equation of Manoussaki et al. (2008) for calculation of low-frequency
461 hearing limit based on the radii ratio (p) of the cochlea: LF = 1.507exp.[−0.578(p-1)].
462

	Equations bases	LF (kHz)	HF (kHz)	Comments
1	Basilar membranous length (BML=cochlear canal length) and number of coiling (N)	0.1219	29.4980	BML= 19.2 mm N= 2.125
2	Basilar membraneous length (BML)	0.3749	31.7227	BML= 19.2 mm
3	Interaural distance (ID) and delay	--	72.9805	ID= 30 mm
4	Radii ratio (p= Rbase/Rapex).	0.5481	--	p= 2.75

463
464 Vestibule of *Ocepeia daouiensis*
465 *Description and comparisons* (Fig. 7)
466 The semicircular canals of *Ocepeia daouiensis* are well developed, but with a low value of **1.42**
467 of the mean SCR (Table 3). Such low SCR value is usually found in small mammals, most
468 having a BM much lower than 1 kg (Spoor et al. 2007; Kemp & Kirk, 2014) (Fig. 8). It means
469 that the semicircular canals are relatively small in *Ocepeia daouiensis* relative to its body size.
470 The ratio of the mean radius (SCR) to the inner ear height (IEH) is 0.25, which supports that the
471 semicircular canals are not reduced relative to the inner ear size by comparison to other placental
472 mammals (e.g., most xenarthrans, litopterns; Billet et al. 2013, 2015).
473 The semicircular canals are noticeably thin with an average thickness ratio of 2.15. In
474 cross-section, the canals have a circular shape. All three semicircular canals display a slight
475 undulation. No ridges were observed on the semicircular canals.

The anterior semicircular canal (ASC) is the largest semicircular canal (Table 3), as most usual in mammals (Cox & Jeffery, 2010) and eutherians (Ekdale & Rowe, 2011), but the difference with the PSC is slight and it is seen mostly in height (=length of some authors). The ASC shape is round. It is slightly curved caudally at the junction of the anterior ampulla. It does not extend much more anteriorly than the anterior ampulla (subvertical connection). The central streamline length of the ASC is 6.87 mm (Table 3) and its average section radius is 0.15 mm. Therefore, the thickness ratio of this canal is 2.22 making it quite slender.

The lateral semicircular canal (LSC) is the smallest semicircular canal (Fig. 7). Its radius of curvature is smaller than those of the anterior and posterior canals (Table 3). The angle of the coiling axis (modiolus) and the LSC is 112.6°. The LSC shape is oval. The slender part of the lateral semicircular canal is connected to the vestibule at a quite high position, above the PSC-vestibule junction and the posterior ampulla. It is partly coalescent with the posterior ampulla and thus forms a partial secondary crus commune. A complete secondary crus commune is known in Cretaceous eutherians, as a plesiomorphic feature (Ekdale & Rowe, 2011). It is also known in several placentals (e.g., Ekdale, 2013), including in afrotherians and paenungulates such as the proboscidean *Phosphatherium* and *Numidotherium*, the sirenian from Chambi, and the macroscelidean *Chambius* (Schmitt & Gheerbrant, 2016; Benoit et al. 2013a, 2013d). The estimated length of the central streamline and the average section radius (0.14 mm) of the lateral canal are similar to the other canals. The thickness ratio of the LSC is slightly lower (2.04) than for the anterior and posterior canals. The LSC is curved dorsally in lateral view, as seen in *Diacodexis* (Ravel & Orliac, 2015). In lateral view the LSC is ventrally canted of about 25° with respect to the skull ventral base (basicranium, esp. basioccipital plane) and skull roof (e.g., sagittal crest) (Fig. 3). The same orientation is observed in the left and right labyrinths, which indicates that it does not result from post-mortem distortion of the petrosals. It means that in *Ocepeia daouiensis,* the head was significantly ventrally tilted when the LSC were horizontal (Fig. 3D). A strongly nose-down head posture with horizontally held LSC is observed in several other mammals such as armadillos (Coutier et al. 2017, Fig. 7) and *Plesiorycteropus* (Benoit et al. 2015b, Fig. 1). Coutier et al. (2017) showed that a high LSC–basicranium angle is also related to some noticeable cranial characters such as strong nuchal crests for strong neck muscles in some xenarthrans, which are indeed also seen in *Ocepeia*. A high LSC –basicranium angle has also been proposed to be linked to a more ground-level based diet in some large mammals (e.g., rhinos in Schellhorn, 2018).

The posterior semicircular canal (PSC) is round (Fig. 7). It extends slightly more distally than the LSC. It also extends in lower position with respect to the LSC (Fig. 7D) by contrast to

eutherians such as zhelestids, but much lower than in advanced paenungulates such as *Procavia*. The posterior arc of the PSC is slightly curved ventrally. The central streamline length is similar to the value found for the anterior canal although slightly longer (7.49 mm). The average section radius is very similar to the anterior one (0.16 mm). Hence the thickness ratio of the posterior canal (2.18) is very close to the ratio of the anterior canal (2.22). The radius of curvature of the posterior canal is 1.25. The PSC does not extend significantly below the LSC.

The anterior and posterior semicircular canals meet high (at approximately 75% of the height of the anterior canal). Hence, the crus commune of the ASC and PSC is elongated (longer than the half height of the PSC), although less long than in generalized eutherians such as zhelestids and *Zalambdalestes* (Ekdale & Rowe, 2011). In lateral view, with the LSC oriented horizontal, the crus commune is noticeably inclined posteriorly as in zhelestid eutherians and in *Protungulatum*; this is a likely plesiomorphic disposition for placentals. The crus commune in *Ocepeia* has no marked basal thickening, and it is smooth without ridges. The average section radius of the *crus commune* of *Ocepeia* is small (0.30 mm) and its length is approximately 1.75 mm. Therefore, *Ocepeia* has a *crus commune* with a relatively low thickness ratio (17.35).

The ampullae of *Ocepeia* are well-defined and inflated (Fig. 7). They are smooth and display no ridges. The anterior ampulla is the most inflated and largest one. There is a distinct canal for nervus ampullaris posterior (a branch of the vestibular nerve), that diverges from the posterior ampulla and is directed anteriorly. It corresponds to the bony channel issued from the foramen singulare.

The angles of semicircular canals in *Ocepeia* do not show strong deviation with respect to the orthogonal orientation (Table 3), as in zhelestids. The greater deviation from the orthogonal orientation is found in the angle between the ASC and LSC (Table 3). We calculated the angle variance index from 90° of the three semicircular canals of *Ocepeia* following Malinzak et al. (2012) and Ruf et al. (2016) as log90 var = 1, 57.

On the vestibule, the spherical recess for the saccule and the elliptical recess for the utricle form quite distinct but connected bulgings below the ASC (Fig. 7C). The condition of *Ocepeia* is similar to *Chriacus*, *Protungulatum* and *Diacodexis* (Bertrand et al. 2019). According to Bertrand et al. (2019) this morphology corresponds to “distinct, but not separated, chambers” of utricle and saccule (their character 15-2). The position of the elliptical recess (and its chamber) for the utricle is closer to the anterior end of the ASC than to its posterior end (character 16-2 in Bertrand et al. 2019).

Table 3a: Dimensions of the semicircular canals of *Ocepeia daouiensis*

Angle ASC/PSC	91.6°
Angle ASC/LSC	80.1°
Angle PSC/LSC	87.8°
Length of crus commune	1.75 mm
Crus commune average section radius	0.30 mm
Crus commune average thickness ratio	17.4

Table 3b: Width (W) and height (H) of the semicircular canals of *Ocepeia daouiensis* (in mm; measurement extending to mid canal section)

	ASC W	ASC H	PSC W	PSC H	LSC W	LSC H
Left labyrinth	3.26	3.01	3.05	2.77	2.38	2.63
Right labyrinth	3.12	3.06	3.05	2.83	2.41	2.61

Table 3c: Radius of curvature and other measurements of the semicircular canals of *Ocepeia daouiensis*. Radius of curvature calculated following the Spoor–Zonneveld equation (Spoor & Zonneveld, 1998): R= ((H+W)/2) x 0.5, with H= height and W = width of the canals

	ASC	PSC	LSC	Mean
Radius of curvature (mean right and left labyrinths; mm)	1.52	1.50	1.25	1.42
Central streamline length (slender part; mm)	6.87	7.49	6.79	7.05
Average thickeness ratio	2.22	2.18	2.04	2.15
Average cross-section diameter	0.15	0.16	0.14	0.15

Functional characters of the semicircular canals of Ocepeia daouiensis

The value of the variance from orthogonality of the semicircular canals in *Ocepeia daouiensis* falls within the range shown by primates with medium head angular velocity magnitude (AVM). However, the poorly known intraspecific variation of the vestibular shape (e.g., Billet et al. 2012; Perier et al. 2016; Gonzales et al. 2019) raises questions on the functional interpretation of the angular variation of the semicircular canals in mammals (Ruf et al. 2016), and especially in fossil taxa. Benson et al. (2016) have also shown that the semicircular canals angles of birds strongly deviate from orthogonality and thus do not follow the trend suggested by Malinzak et al. (2012) for agile mammal taxa. Hence, the variation of the SC deviation from orthogonality certainly requires further study in extant mammals before stating on its potential functional meaning.

Table 4. Body mass estimates of *Ocepeia daouiensis* in grams (*mean of upper and lower teeth; **estimation = minimal size). Predictive allometric equations from Damuth (1990), Damuth & MacFadden (1990) for all ungulates, selenodonts, and selenodont browsers. The best estimates (see Gheerbrant et al. 2014) are in bold (mean for all ungulates = 3.5 kg; see text).

Measurements base	All ungulates	Selenodonts	Selenodont browsers
Area M1*	9306,15	8769,99	7881,27
Area M2*	7556,50	7130,07	6358,69
Area M3*	5756,35	5188,77	4830,70
Length M1*	6924,72	6934,83	6357,63
Length M2*	4394,59	4037,88	3691,52
Length M3*	**3484,46**	**2741,06**	**2687,64**
Length M1-3*	**4043,51**	**3846,18**	**3417,84**
Skull length**	**2950,34**	--	--

Spoor et al. (2007) have proposed a link between the agility of mammals and the size of their semicircular canals (radius of curvature, SCR) relative to their body mass. They designed predictive equations of agility categories ("agility score") that could be used to infer the locomotory behaviour of extinct taxa (see also Silcox et al. 2009). However, criticism has been expressed on the subjectivity of the defined agility categories, on the weakness of the link between SCR and agility and on the simplistic view that one morphological parameter of the SC could suffice to predict agility (e.g., David et al. 2010, 2016; Malinzak et al. 2012). The significance of the "agility score" inferred from the semicircular canals size is indeed debated

and challenged (Graf & Klam, 2006; Kemp & Kirk, 2014; David et al. 2016; Benson et al. 2017; Gonzales et al. 2019). In particular, Kemp & Kirk (2014) evidenced a more significant relation of the variance of the semicircular canal size with those of the eye size and visual acuity. They showed that once variance linked to body mass is removed, larger semicircular canals are found in mammals with large eyes and higher visual acuity.

For these reasons, we do not discuss the significance for locomotion of the "agility scores" calculated for *Ocepeia daouiensis* (Fig. 8). Instead, we plotted the mean radius of curvature of the semicircular canals (SCR) and the body mass (BM in grams) in a graph containing a wealth of mammalian species as previously studied and figured by Spoor et al. (2007). The mean body mass of *Ocepeia daouiensis* was estimated as 3.5 kg (Table 4) based on the length of M1-3, of M3 and of the skull (Gheerbrant et al. 2014). In the graph depicted in figure 8, *Ocepeia* plots at very low SCR values, close to extant sloths. For the sake of comparison, we added several extant afrotherians to the Spoor et al. (2007) dataset. It shows that the insectivore-like afrotherians such as tenrecs and golden moles (tenrecoideans) share with *Ocepeia* a small labyrinth with respect to other mammals with similar body mass. This shows that both *Ocepeia* and some tenrecoideans share small semicircular canals relative to their body mass, and in fact also small inner ears and petrosals (at least for *Ocepeia*, see above). It is difficult to evaluate the size of the eyes in *Ocepeia*, but a gross estimate based on the morphology and relative size of the orbit (Gheerbrant et al. 2014), as preserved in MNHN.F.PM45, indicates rather small eyes relative to body mass (Kemp & Kirk, 2014, table 1), with an estimated eye diameter around 15 mm. *Ocepeia* seems indeed to fit well with Kemp and Kirk's (2014) model that links relatively reduced semicircular canals and small eyes. The distribution of the small eyes character state in afrotherians and its phylogenetic significance remain to be investigated.

Discussion

One remarkable feature of *Ocepeia* is the small size of its petrosal (pars cochlearis and pars canalicularis) and inner ear with respect to the skull and body size. The significance of a small petrosal remains poorly known. However, and interestingly, we found that the semicircular canals are also relatively small in tenrecoidean afrotherians which might be a shared phylogenetic feature. A relatively small petrosal and labyrinth may be original and derived within placentals, although more investigation is needed within this group. Its evolutionary state within afrotherians remains uncertain (see below).

Our comparisons evidence the mostly plesiomorphic morphology of the petrosal of *Ocepeia* among placentals, especially for the labyrinth; most noticeable symplesiomorphies are reported in Table 5. This is congruent with the skull morphology of *Ocepeia* (Gheerbrant et al. 2014) that resembles the stem eutherian pattern in many characters.

The ancestral morphotype of the bony labyrinth of the Afrotheria and Paenungulata was previously characterized based on extant species (Ekdale, 2013). Recent important fossil discoveries in the Paleogene of Africa provided new key data on the morphology of early afrotherians, especially with the Selandian and Ypresian proboscideans *Eritherium* and *Phosphatherium* (Schmitt & Gheerbrant, 2016), the early/middle Eocene hyracoid *Seggeurius* (Benoit et al. 2015a), the unnamed early/middle Eocene sirenian from Chambi (Benoit et al. 2013a), the early/middle Eocene macroscelidean *Chambius* (Benoit et al. 2013b), and the Oligocene embrithopod *Arsinoitherium* (Benoit et al. 2013c). The paenungulatomorph *Ocepeia* (Gheerbrant et al. 2014) adds to these early taxa and further helps to enlighten the ancestral labyrinthine morphology of the Paenungulata. It confirms several ancestral features inferred by Ekdale (2013) (Table 5: 1, 2, 7, 9) for the afrotherians. However, it also shows that the afrotherian and paenungulatomorph labyrinth morphotypes were closer to the eutherian morphotype in several characters listed in Table 5. In particular, the relative cochlear volume (Table 5: 8) is greater in *Ocepeia* (66%) than in the ancestral morphotype reconstructed by Ekdale (2013) for paenungulates (56 %), afrotherians (56 %) and placentals (58%). It is actually close to the Afroinsectiphilia (64% in Ekdale, 2013), and to stem eutherians, which could support it is a generalized feature of the Afrotheria. Another noticeable plesiomorphic trait present in *Ocepeia* is the posteriorly inclined crus commune (Table 5: 6).

With respect to eutherians and afrotherians, few specialized features are identified in *Ocepeia*. The angle of the cochlea and LSC planes is larger in *Ocepeia* (60-50°) than in zhelestids (29°-41°), but it remains still smaller with respect to most placentals. The aspect ratio

of the cochlea of *Ocepeia* (0.72) is higher than in non-placental eutherians, several early placentals such as *Protungulatum* and *Alcidedorbignya,* and several paenungulates, including early taxa such as *Eritherium* (0.35), *Numidotherium* (0.51), *Seggeurius* (0.48), and *Arsinoitherium* (0.45). It is close or identical to *Chambius,* the sirenian from Chambi, and *Moeritherium,* as a likely convergence. The incomplete separation of the posterior arm of the LSC with the PSC is derived with respect to the true secondary crus commune known in eutherians and also in afrotherians and paenungulates (e.g., *Phosphatherium*, *Numidotherium*, the sirenian from Chambi, *Orycteropus* and *Chambius*). *Ocepeia* has an intermediate state of the relative position of the PSC and LSC: the posterior arm of the PSC enters the vestibule in lower position with respect to the LSC plane than in eutherians, but it is even lower in more derived placental taxa such as *Procavia*. The cochlea of *Ocepeia* is slightly more coiled than in some early paenungulates such as *Seggeurius* (688°) and *Numidotherium* (540 to 584°) and several extant afrotherians (Ekdale, 2013). However, this character is subject to significant individual variation (e.g., Schmitt 2016) which reduces its phylogenetic value. The large and inflated tegmen tympani is derived with respect to stem eutherians and it is a remarkable shared trait with paenungulates (Schmitt & Gheerbrant, 2016). However, this trait is known in other placentals. A large and/or inflated tegmen tympani is known in some early euungulates (Ciffelli, 1982), artiodactyls (O'Leary, 2010) and some South American extinct euungulates such as litopterns and notoungulates (Billet et al 2015; Billet & Muizon 2013). It is unknown 1) if the state is exactly homologous in these taxa, and 2) if this is a convergent trait of the Paenungulatomorpha and other placentals. The distribution of this feature and its states among placentals actually need to be further investigated. Similarly, the large and distally extended mastoid process is derived with respect to eutherians. A large mastoid process is also known in proboscideans (Gheerbrant et al. 2005), but the distribution of this feature within other Paenungulata remains poorly known. A remarkable feature of *Ocepeia* is the dorsoventral orientation of the large canal for the ramus superior. It may represent a derived feature, although here again it remains to be investigated in a larger sample of extinct and extant placentals. The thick medial caudal tympanic process described in *Ocepeia* is shared with *Seggeurius* in which it is called "a swelling on the septum metacochleare" (Benoit et al. 2015a). The latter was interpreted as a possible synapomorphy of the Sirenia and Hyracoidea (Benoit et al. 2015a). Its presence in *Ocepeia* argues for a more generalized feature within paenungulatomorphs. Finally, the distinct but still connected chambers of the utricle and saccule and the position of the utricle closer to anterior end of ASC seen in *Ocepeia* correspond to two derived features within placentals according to Bertrand et al. (2019; characters 15-2, 16-2). They suggested that these two traits support relationships of

682 *Chriacus* with crown euungulates such as the Artiodactyla. Nevertheless, *Ocepeia* demonstrates
683 a wider distribution of these features among placentals which are occurring at least in
684 paenungulatomorphs and euungulates.
685 The relatively small petrosal (pars cochlearis and pars canalicularis) and its labyrinth might
686 be a basal afrotherian synapomorphy retained in tenrecoideans and in *Ocepeia*, and lost in crown
687 paenungulates and in other afroinsectiphilians. This hypothesis is favoured against the alternative
688 one of an exclusive synapomorphy of the tenrecoideans and *Ocepeia* because it is consistent with
689 the paenungulates relationships of *Ocepeia* (clade Paenungulatomorpha) supported by a large set
690 of other craniodental features (Gheerbrant et al. 2014, 2016, 2018). The distribution among
691 placentals of a relatively small labyrinth and petrosal as seen in *Ocepeia,* and its phylogenetic
692 significance remain, however, to be investigated in a cladistic analysis.
693 Several plesiomorphic traits of *Ocepeia* are also found in early crown paenungulates
694 (Table 5: 1, 2-5, 8-11, 15, 18). The petrosal and bony labyrinth of early crown paenungulates is
695 as a whole poorly specialized with respect to known stem paenungulates (paenungulatomorphs)
696 such as *Ocepeia*. This is especially true for the earliest known one, *Eritherium* (Schmitt &
697 Gheerbrant, 2016).
698

Table 5. Plesiomorphic features of *Ocepeia*, with indication of the putative ancestral morphotype taxonomic rank and primary reference inferring character polarity within mammals. References: (1) Billet et al. (2015), (2) Billet et Muizon (2013), (3) Coutier et al. (2017), (4) Ekdale (2013), (5) Ekdale & Rowe (2011), (6) Gheerbrant et al. (2014), (7) Macrini et al. (2007), (8) Macrini et al. (2010), (9) Macrini et al. (2013), (10) Meng & Fox (1995), (11) Muizon et al. (2015), (12) Orliac & O'Leary (2016), (13) Schmitt & Gheerbrant (2016).

#K	Structure	Character states seen in *Ocepeia*	Hypothetical ancestral morphotype	References
1	Labyrinth	Largest SC: ASC	Theria, Eutheria	(1) (4) (9)
2	Labyrinth	Thin semicircular canals	Theria, Eutheria	(1) (13)
3	Labyrinth	High Crus Commune	Eutheria	(5)
4	Labyrinth	Ampulla well inflated	Theria, Eutheria	(5)
5	Labyrinth	Crus Commune posteriorly canted, far from anterior ampulla	Theria?, Eutheria	(12)
6	Labyrinth	Cochlea with 2 turns (765°)	Placentalia convergences	(5) (10)
7	Labyrinth	Cochlea vs labyrinth volume > 64 %	Theria, Eutheria	(4)
8	Labyrinth	Closed angle of cochlea and LSC planes	Theria, Eutheria	(12)
9	Labyrinth	Secondary bony lamina present, extended on all cochlea first turn	Theria, Eutheria, Placentalia?	(1)(10) (13)
10	Labyrinth	High stapedial ratio (H>1.7)	Eutheria	(8)
11	Labyrinth	Aq. vestibuli located antero-medial to the crus commune	Eutheria?, Placentalia	(12)
12	Labyrinth	Aq. cochlearis posteriorly oriented	Eutheria?	(12)
13	Labyrinth	Fen. vestibuli far ventrally from lateral ampulla	Eutheria?	(12)
14	Labyrinth	Fen. vestibuli large (but smaller than external aperture of the cochlear fossula)	Eutheria	(13)
15	Labyrinth	Spiral turns of cochlea loosely connected	Eutheria, Placentalia?	(11)
16	Petrosal	Large and inflated tegmen tympani	Paenungulatomorpha? But also known in euungulates such as *Meniscotherium*, artiodactyls, litopterns, notoungulates (convergences?)	(6)
17	Petrosal	tegmen tympani pierced by a large canal for the ramus superior	Eutheria, Placentalia?	(1) (2) (11)
18	Petrosal	Deep and rounded fossa subarcuata	Theria, Eutheria	(1) (7) (13)

Conclusion

The labyrinth morphology indicates that *Ocepeia* has a nose-down head posture when the LSC is held horizontally. The functional study of the cochlea evidences a higher sensitivity for low frequency sounds and a lower sensitivity for high frequency sounds of the hearing of *Ocepeia* with respect to Cretaceous eutherians. The petrosal of *Ocepeia* shows some remarkable traits such as its relatively small pars cochlearis, pars canalicularis, and labyrinth (esp. SCs), a large wing-like pars mastoidea, a large and inflated tegmen tympani, and the dorsoventral orientation of the large canal for the ramus superior. The relative small size of the SCs and petrosal is shown to be an interesting shared trait with tenrecoidean afrotherians.

Ocepeia further shows that the ancestral morphotype of the petrosal and labyrinth in the Paenungulatomorpha retained many plesiomorphic features of the generalized eutherian pattern. This is in fact true for the whole skull morphology of *Ocepeia* (Gheerbrant et al. 2014). It is also consistent with the plesiomorphic morphology of the earliest known proboscidean *Eritherium* found in the same Selandian Ouled Abdoun phosphate beds (Gheerbrant, 2009; Schmitt & Gheerbrant, 2016). In this regard *Ocepeia* is among the very few available fossils documenting morphological features at the base of the Paenungulata and Afrotheria that should help to further test the relationships of the major clades diverging at the placental root, which are currently mostly based on molecular data (e.g., Madsen et al. 2001; Murphy et al. 2001; Springer et al. 2004; Foley et al. 2016). The formal phylogenetic significance of the labyrinthine features of early crown and stem paenungulates such as *Ocepeia* remains to be tested with a phylogenetic analysis.

Acknowledgements

We thank Romain David for discussion and use of the software Ariadne. We thank Miguel Garcia Sanz (MNHN, AST-RX platform) for producing the CT scans and Florent Goussard and Nathalie Poulet (CR2P) for assistance with 3D digital reconstructions and imaging based on CT scans, and also for measurements on CT scan images and 3 D digital models. Silhouettes images were downloaded from the PhyloPic website. We thank the three reviewers and the editor who helped to improve our manuscript.

References

Benoit J, Adnet S, El Mabrouk E, et al. (2013a) Cranial Remain from Tunisia Provides New Clues for the Origin and Evolution of Sirenia (Mammalia, Afrotheria) in Africa. *PLoS ONE* 8(1): e54307. doi:10.1371/journal.pone.0054307.

Benoit J, Crumpton N, Merigeaud S, et al. (2013b) Petrosal and bony labyrinth morphology supports paraphyly of *Elephantulus* within Macroscelididae (Mammalia, Afrotheria). *J Mammal Evol* 21, 173-193. DOI:10.1007/s10914-013-9234-5.

Benoit J, Merigeaud S, Tabuce R (2013c) Homoplasy in the ear region of Tethytheria and the systematic position of Embrithopoda (Mammalia, Afrotheria). *Geobios* 46: 357-370. http://dx.doi.org/10.1016/j.geobios.2013.07.002

Benoit J, Orliac M, Tabuce R (2013d) The petrosal of *Chambius* (Macroscelidea, Afrotheria) from the Eocene of Djebel Chambi (Tunisia) and the evolution of the ear region in elephant shrews. *J Syst Pal* 11, 907-923. DOI:10.1080/14772019.2012.713400.

Benoit, J, Crochet, J-Y, Mahboubi, M, et al (2015a) New material of *Seggeurius amourensis* (Paenungulata, Hyracoidea), including a partial skull with intact basicranium. J Vert Pal 36, e1034358. DOI: 10.1080/02724634.2015.1034358.

Benoit J, Lehmann T, Vatter M, et al. (2015b) Comparative anatomy and three-dimensional geometric morphometric study of the bony labyrinth of Bibymalagasia (Mammalia, Afrotheria). *J Vert Pal* 35 (3), e930043.

Benson RBJ, Starmer-Jones E, Close RA, et al (2017) Comparative analysis of vestibular ecomorphology in birds. *J Anat* 231, 990 – 1018.

Bertrand OC, Shelley SL, Wible JR, et al (2019) Virtual endocranial and inner ear endocasts of the Paleocene 'condylarth' *Chriacus*: new insight into the neurosensory system and evolution of early placental mammals. *J Anat*, https://doi.org/10.1111/joa.13084.

Billet G, Muizon CD, (2013). External and internal anatomy of a petrosal from the late Paleocene of Itaboraí, Brazil, referred to Notoungulata (Placentalia). J Vert Pal 33, 455–469. https://doi.org/10.1080/02724634.2013.722153

Billet G, Hautier L, Asher RJ, et al. (2012) High morphological variation of vestibular system accompanies slow and infrequent locomotion in three-toed sloths. *Proc R Soc B* 279, 3932–3939.

780 **Billet G, Germain D, Ruf I, et al.** (2013) Inner ear morphology in *Megatherium* and
781 insights on the evolution of vestibular system and locomotion in sloths. *J Anat*
782 223, 557–567.

783 **Billet G, de Muizon C, Schellhorn R, et al. (**2015) Petrosal and inner ear anatomy
784 and allometry amongst specimens referred to Litopterna (Placentalia). *Zool J*
785 *Linn Soc* 173, 956–987.

786 **Cameron J, Shelley S L, Williamson T E, et al.** (2019) The Brain and Inner Ear of
787 the Early Paleocene "Condylarth" *Carsioptychus coarctatus*: Implications for
788 Early Placental Mammal Neurosensory Biology and Behavior. *Anat Rec*
789 302(2), 306-324.

790 **Cifelli LR** (1982) The petrosal structure of *Hyopsodus* with respect to that of some other
791 ungulates, and its phylogenetic implications. *J Paleont* 56, 795–805.

792 **Court N** (1992) Cochlea anatomy of *Numidotherium koholense*: auditory acuity in
793 the oldest known proboscidean. *Lethaia* 25, 211-215.

794 **Coutier F, Hautier L, Cornette R, et al.** (2017) Orientation of the lateral semicircular
795 canal in Xenarthra and its links with head posture and phylogeny. *J Morph* 278 (5),
796 704–717.

797 **Cox PG, Jeffery N** (2010) Semicircular canals and agility: The influence of size
798 and shape measures *J Anat* 216, 37–47.

799 **Damuth J** (1990). Problems in estimating body masses of archaic ungulates using dental
800 measurements. In *Body size in mammalian paleobiology: estimation and biological*
801 *implications* (eds Damuth J, MacFadden BJ, pp 229–253. New York: Cambridge
802 University Press.

803 **Damuth J, MacFadden B J** (1990) *Body Size in Mammalian Paleobiology.* Cambridge:
804 Cambridge University Press.

805 **David R, Droulez J, Allain R, et al.** (2010). Motion from the past. A new method to infer
806 vestibular capacities of extinct species. *C R Palevol* 9, 397–410.

807 **David R, Stoessel A, Berthoz A, et al.** (2016) Assessing morphology and function of the
808 semicircular duct system: introducing new in-situ visualization and software toolbox.
809 *Sci Rep* **6**, 32772.

810 E**kdale EG** (2013) Comparative anatomy of the bony labyrinth (inner ear) of placental
811 mammals. *PLoS One* 8 (e66624), 1–100.

812 **Ekdale EG, Rowe T** (2011) Morphology and variation within the bony labyrinth of
813 zhelestids (Mammalia, Eutheria) and other therian mammals. *J Vert Pal* 31, 658-675.

814 **Evans H E, de Lahunta A (2012).** *Miller's Anatomy of the Dog.* St Louis: Saunders.

Foley N M, Springer M S, Teeling E C (2016) Mammal madness: is the mammal tree of life not yet resolved? *Philosophical Transactions of the Royal Society B*: Biological Sciences, 371(1699), 20150140.

Gheerbrant E, (2009) Paleocene emergence of elephant relatives and the rapid radiation of African ungulates: Proc Natl Acad Sci 106, 10717–10721**.**

Gheerbrant E (2010). Primitive African ungulates ("Condylarthra" and Paenungulata). In *Cenozoic Mammals of Africa* (eds Werdelin L., Sanders W.J.), p. 563-571. Berkeley, Los Angeles, London: The University of California Press.

Gheerbrant E, Sudre J, Tassy P, Amaghzaz M, Bouya B, Iarochene M, (2005). Nouvelles données sur *Phosphatherium escuilliei* (Mammalia, Proboscidea) de l'Eocène inférieur du Maroc, apports à la phylogénie des Proboscidea et des ongulés lophodontes. Geodiversitas 27, 239–333.

Gheerbrant E, Amaghzaz M, Bouya B, et al. (2014) *Ocepeia* (middle Paleocene of Morocco): the oldest skull of an afrotherian mammal. *PLOS One* **9**(2), 1-30 (DOI: 10.1371/journal.pone.0089739).

Gheerbrant E, Filippo A, Schmitt A (2016) Convergence of Afrotherian and Laurasiatherian Ungulate-Like Mammals: First Morphological Evidence from the Paleocene of Morocco. *PLoS ONE* **11**(7), 1-35. Doi:10.1371/journal.pone.0157556.

Gheerbrant E, Schmitt A, Kocsis L (2018) Early African Fossils Elucidate the Origin of Embrithopod Mammals. *Cur Biol* **28** (19), 2167-2173.

Gonzales L A, Malinzak M D, Richard F K (2019) Intraspecific variation in semicircular canal morphology—A missing element in adaptive scenarios? *Am J Phys Anthropol*, 168, 10–24.

Graf W, Klam F (2006) Le système vestibulaire: anatomie fonctionnelle et comparée, évolution et développement. *C R Palevol* 5 (3–4): 637-655.

Gunz P, Ramsier M, Kuhrig M, et al. (2012) The mammalian bony labyrinth reconsidered, introducing a comprehensive geometric morphometric approach. *J Anat* 6: 529–543.

Harper T, Rougier G (2018) Petrosal morphology and cochlear function in Mesozoic stem therians. bioRxiv preprint, online Dec. 7, 2018; doi: http://dx.doi.org/10.1101/490367

Heffner RS, Heffner HE (2008) *High-frequency hearing. In Handbook of the senses: audition* (eds Dallos P, Oertel D, Hoy R), p. 55–60. New York: Elsevier.

Kemp AD, Kirk EC (2014) Eye size and visual acuity influence vestibular anatomy in mammals. *Anat Rec* 297, 781–790.

Kirk EC, Gosselin-Ildari AD (2009) Cochlear labyrinth volume and hearing abilities in primates. *Anat Rec* 292, 765–776.

Kocsis L, Gheerbrant E, Mouflih M, et al. (2014) Comprehensive stable isotope investigation of marine biogenic apatite from the late Cretaceous—early Eocene phosphate series of Morocco. *Palaeogeogr, Palaeoclim, Palaeoecol* 394, 74–88.

MacPhee RDE (1981) Auditory regions of primates and eutherian insectivores. Morphology, ontogeny, and character analysis. *Contribution to Primatology* 18, 1, 1-284.

Macrini TE, Rougier GW, Rowe T (2007) Description of a cranial endocast from the fossil mammal *Vincelestes neuquenianus* (Theriiformes) and its relevance to the evolution of endocranial characters in therians. *Anat Rec* 290, 875–892. (doi:10.1002/ar.20551)

Macrini TE, Flynn JJ, Croft DA, et al. (2010) Inner ear of a notoungulate placental mammal: anatomical description and examination of potentially phylogenetically informative characters. *J Anat* 216, 600-610.

Macrini TE, Flynn J J, Ni X, et al. (2013) Comparative study of notoungulate (Placentalia, Mammalia) bony labyrinths and new phylogenetically informative inner ear characters. *J Anat* 223(5), 442-461.

Madsen O, Scally M, Douady CJ, et al. (2001) Parallel adaptive radiations in two major clades of placental mammals. *Nature* 409, 610–614.

Malinzak MD, Kay RF, Hullar TE (2012) Locomotor head movements and semicircular canal morphology in primates. *Proc Natl Acad Sci USA* 109, 17914–17919.

Manoussaki D, Chadwick RS, Ketten DR, et al (2008) The influence of cochlear shape on low-frequency hearing. *Proc Natl Acad Sci USA*, 105, 6162-6166.

Meng J, Fox RC (1995) Osseous inner ear structures and hearing in early marsupials and placentals. *Zool J Lin Soc* 115, 47-71.

Muizon C de, Billet G, Argot C, et al. (2015) *Alcidedorbignya inopinata,* a basal pantodont (Eutheria, Mammalia) from the early Palaeocene of Bolivia: anatomy, phylogeny, and palaeobiology. *Geodiv* 37 (4), 397–634. https://doi.org/10.5252/g2015n4a1

Murphy W J, Eizirik W E, Johnson E, et al. (2001) Molecular phylogenetics and the origins of placental mammals. *Nature* 409: 614–618.

Nowak R M (1999) Walker's Mammals of the World. 6th Edition.

O'Leary M A (2010) An anatomical and phylogenetic study of the osteology of the petrosal of extant and extinct artiodactylans (Mammalia) and relatives. *Bull Am Mus Nat Hist* 335, 1-206

Orliac M J, Benoit J, O'Leary M A (2012) The inner ear of *Diacodexis*, the oldest artiodactyl mammal. *J Anat* 221, 417–426

Orliac M J, O'Leary M A (2016) The inner ear of *Protungulatum* (Pan-Euungulata, Mammalia). *J Mammal Evol* 23, 4, 337–352.

Perier A, Lebrun R, Marivaux L (2016) Different level of intraspecific variation of the bony labyrinth morphology in slow-versus fast-moving primates. *J Mammal Evol* 23, 353–368.

Ravel A, Orliac M (2015) The inner ear morphology of the 'condylarthran' *Hyopsodus lepidus*. *Hist Biol* 27, 957-969.

Rosowski JJ (1992) Hearing in transitional mammals: Predictions from the middle-ear anatomy and hearing capabilities of extant mammals. In *The evolutionary biology of hearing* (eds Webster DB, Fay RR, Popper AN), pp. 615-631. New York: Springer.

Rosowski JJ, Graybeal A (1991) What did *Morganucodon* hear? *Zool J Linn Soc* 101(2), 131–168. doi:10.1111/j.1096-3642.1991. tb00890.x

Ruf I, Volpato V, Rose KD, et al. (2016) Digital reconstruction of the inner ear of *Leptictidium auderiense* (Leptictida, Mammalia) and North American leptictids reveals new insight into leptictidan locomotor agility. *Paläontol Z* 90(1), 153–171. doi:10.1007/s12542-015-0276-2.

Schellhorn R (2018) A potential link between lateral semicircular canal orientation, head posture, and dietary habits in extant rhinos (Perissodactyla, Rhinocerotidae). *J Morph* 279 (1), 50 – 61.

Schmitt A (2016) La région de l'oreille osseuse chez les Proboscidea (Afrotheria, Mammalia): anatomie, fonction, évolution, Doctoral dissertation, Paris, Muséum national d'histoire naturelle.

Schmitt A, Gheerbrant, E (2016) The ear region of earliest known elephant relatives: new light on the ancestral morphotype of proboscideans and afrotherians. *J Anat* 228, 137-152.

Schmelzle T, Sánchez−Villagra MR, Maier W (2007) Vestibular labyrinth diversity. *Mammal Study* 32, 83-97.

Segall W (1970) Morphological parallelisms of the bulla and auditory ossicles in some insectivores and marsupials. *Fieldiana Zool* 51, 169-205

Silcox M.T, Bloch J.I, Boyer D.M, et al. (2009). Semicircular canal system in early primates. *J Hum Evol* 56, 315-327.

Spoor F, Garland T, Krovitz G, et al. (2007) The primate semicircular canal system and locomotion. *Proc Natl Acad Sci USA* 104, 10808-10812.

Spoor F, Zonneveld F (1998) Comparative review of the human bony labyrinth. *Am J Phys Anthropol* 107, 211-251.

Springer MS, Stanhope MJ, Madsen O, et al. (2004). Molecules consolidate the placental mammal tree. *Trends Ecol Evol* 19, 430–438.

Waibl H, Gasse H, Constantinescu GM, et al. (2005) *Nomina Anatomica Veterinaria*. 5th ed. Hannover, Germany ; Columbia, MO, USA ; Ghent, Belgium: Editorial Committee.

West CD (1985) The relationship of the spiral turns of the cochlea and the length of the basilar-membrane to the range of audible frequencies in ground dwelling mammals. *J Acoust Soc Am* 77, 1091-1101.

Wible JR (1993) Cranial circulation and relationships of the colugo *Cynocephalus* (Dermoptera, Mammalia). *American Museum Novitates* **3072**, 1-27.

Wible JR (2008) On the Cranial Osteology of the Hispaniolan Solenodon, *Solenodon paradoxus* Brandt, 1833 (Mammalia, Lipotyphla, Solenodontidae). *Ann Carn Mus* **77**, 321-402. doi:10.2992/0097-4463-77.3.321.

Wible JR (2010) Petrosal anatomy of the nine-banded armadillo, *Dasypus novemcinctus* Linnaeus, 1758 (Mammalia, Xenarthra, Dasypodidae). *Ann Carn Mus* **79**, 1–29.

Wible JR, Rougier GW, Novacek MJ, et al. (2009) The Eutherian Mammal *Maelestes gobiensis* from the Late Cretaceous of Mongolia and the phylogeny of cretaceous eutheria. *Bulletin of the American Museum of Natural History* **2009**, 1. doi:10.1206/623.1.

Wible JR, Rougier GW, Novacek MJ, et al. (2001) Earliest eutherian ear region: a petrosal referred to *Prokennalestes* from the early Cretaceous of Mongolia. *Am Mus Nov, New York,* **3322**, 1-44.

Yans J, Amaghzaz M, Bouya B, et al. (2014) First carbon isotope chemostratigraphy of the Ouled Abdoun phosphate Basin, Morocco; implications for dating and evolution of earliest African placental mammals. *Gondwana Res* 25, 257–269.

Zack SP, Rose KD, Holbrook LT, et al 2019. An enigmatic new ungulate-like mammal from the early Eocene of India. *Papers in Palaeontology* n/a. https://doi.org/10.1002/spp2.1288

Caption and list of figures

Fig. 1. Simplified cladogram showing the phylogenetic relationships of *Ocepeia* within Afrotheria (after Gheerbrant et al. 2014, 2016, 2018).

Fig. 2. Measurement protocol of the endocast of the inner ear of *Ocepeia daouiensis*.

(**A**) stapedial ratio (L = length, W = width); (**B**) cochlear aspect ratio (H = heigth, W = width): (**C**) anterior semicircular canal central streamline length, (**D**) lateral semicircular canal central streamline length; (**E**) posterior semicircular canal central streamline length: (**F**) cochlear length; (**G**) length (ASCL) and width (ASCW) of the anterior semicircular canal used to calculate the radius of curvature; (**H**) length (LSCL) and width (LSCW) of the lateral semicircular canal used to calculate the radius of curvature.

Fig. 3. 3D digital model of the skull MNHN.F.PM45 of *Ocepeia daouiensis* showing by transparency the petrosal and labyrinth, and the skull posture with the lateral semicircular canal horizontally held (E, F, G).

(**A-B**), ventral views: A, modeling of the petrosals (yellow); B, modeling of the petrosals (transparent, yellow) and labyrinths (red). (**C-D**), right lateral view with the lateral semicircular canal (SCL) horizontally held: C, modeling of the petrosals (yellow); D, modeling of the petrosals (transparent, yellow) and labyrinths (red). This figure displays the relative small size of the inner ear in the petrosal of *Ocepeia daouiensis*, the large extent of the mastoid part of the petrosal within the skull and the ventrally inclined posture of the skull in C-D (SCL horizontal).

Fig. 4. 3D digital model of the petrosals of *Ocepeia daouiensis,* skull specimen MNHN.F.PM45.

(A), anterior view; (**B**), ventral view; (**C**), ventromedial view. Scale-bar: 4mm.

Abbreviations: aav, external aperture of the vestibular aqueduct; ab. X n.?, possible notch/sulcus for the auricular branch of the vagus nerve (X); acan n, notch housing the external aperture of the cochlear canaliculus; acf, external aperture of the cochlear fossula; br., broken area; cp, crista parotica; fai, foramen acusticum inferius; fas, foramen acusticum superius; fi, fossa incudis; fs, facial sulcus; fsa, fossa subarcuata; fv, fenestra vestibuli; hf, hiatus Fallopii; iam, internal auditory meatus; ips, sulcus for the inferior petrosal sinus; mctp, medial caudal tympanic process; mfe, medial flattened edge; mp, mastoid part of the petrosal; pfc, prefacial commissure; pps, postpromontorial tympanic sinus; pts?, possible postemporal sulcus; rsup c, canal for the ramus superior (of the

stapedial artery); rtp, rostral tympanic process; sff, secondary facial foramen; smn, stylomastoid notch; ttf, tensor tympani fossa; stf, stapedial fossa; stb?, possible sulcus for temporal branch; stf, stapedial fossa; thyl, tympanohyal; tt, tegmen tympani.

Fig. 5. 3D digital model of the petrosals of *Ocepeia daouiensis,* skull specimen MNHN.F.PM45.

(**A**), lateral view; (**B**), lateral view with transparency of the petrosal, and with the canal for the ramus superior of the stapedial artery highlighted; (**C**), cerebellar view; (**D**), dorsal view. Scale-bar: 4mm

Abbreviations: aav, external aperture of the vestibular aqueduct; ab. X n.?, possible notch/sulcus for the auricular branch of the vagus nerve (X); acan n, notch housing the external aperture of the cochlear canaliculus; acf, external aperture of the cochlear fossula; br., broken area; cp, crista parotica; er, epitympanic recess; fai, foramen acusticum inferius; fas, foramen acusticum superius; fi, fossa incudis; fs, facial sulcus; fsa, fossa subarcuata; fv, fenestra vestibuli; hf, hiatus Fallopii; iam, internal auditory meatus; ips, sulcus for the inferior petrosal sinus; mctp, medial caudal tympanic process; mfe, medial flattened edge; mp, mastoid part of the petrosal; pfc, prefacial commissure; pps, postpromontorial tympanic sinus; pts?, possible postemporal sulcus; rsup c, canal for the ramus superior (of the stapedial artery); rtp, rostral tympanic process; sff, secondary facial foramen; stb?, possible sulcus for temporal branch; stf, stapedial fossa; ttf, tensor tympani fossa; thyl, tympanohyal; tt, tegmen tympani.

Fig. 6. 3D digital model of the petrosals of *Ocepeia daouiensis,* specimen MNHN.F.PM45, with the labyrinth by transparency.

(**A**), right petrosal in cerebellar view; (**B**), left petrosal in cerebellar view; (**C**), right petrosal in anterior view; (**D**), left petrosal in anterior view; (**E**), right petrosal in tympanic view; (**F**), left petrosal in tympanic view. In red the labyrinth, in green the canal for the ramus superior (of the stapedial artery) within the tegmen tympani. Scale-bar: 4mm

Fig. 7. 3D reconstructed digital model of the left bony labyrinth *of Ocepeia daouiensis*, specimen MNHN.F.PM45.

(**A**) dorsal view, (**B**) anterior view, (**C**) medial view, (**D**) ventral view and (**E**) medio-anterior view.

Abbreviations: **aa** anterior ampulla, **asc** anterior semicircular canal, **av** *aquaeductus vestibuli*, **cc** *crus commune*, **cca** cochlear canaliculus, **co** cochlea, **er** elliptical recess, **fc**

fenestra cochleae, **fv** *fenestra vestibuli*, **la** lateral ampulla, **lsc** lateral semicircular canal, **pa** posterior ampulla, **psc** posterior semicircular canal, **sbl**, secondary bony lamina, **sr**, spherical recess, **va**, vestibular aqueduct. Orientation axes: dors dorsal; md medial, lat lateral, post posterior.

Fig. 8. Graphical relationship between the size of the semicircular canals (SCR, radius of curvature) versus body-mass (BM), with the indication of agility estimates in various mammals as measured and compiled by Spoor et al. (2007). Measurements for *Ocepeia daouiensis*, and several extant afrotherians such *Orycteropus*, *Macroscelides*, *Rhynchocyon*, *Procavia*, *Dendrohyrax*, *Potamogale*, *Tenrec*, *Tenrec*, *Chrysochloris*, *Hemicentetes* were added to the dataset (silhouettes from PhyloPic website) (see SuppData S3). This diagram shows that *Ocepeia* and the insectivore-like afrotherians (Tenrecoidea) are characterized by a relative small size of the semicircular canals with respect to other mammals of the same body mass.

Caption of Tables

Table 1. Measurements of the cochlea and fenestrae of the bony labyrinth of *Ocepeia daouiensis* (mm)

Table 2. Estimation of the hearing frequency range of *Ocepeia* based on its labyrinth dimensions. LF: Low-frequency limit; HF: High-frequency limit. 1. Equation of West (1985), Meng & Fox (1995), based on basilar membranous length (BML=cochlear canal length) and number of coiling (N); Frequency limits at 60 dB Sound Pressure Level: log(LF) = 1.76-1.66 log(BMLxN); log(HF) = 2.42-0.994 log(BML/N). 2. Equation of Rosowski and Graybeal (1991) and Rosowski (1992), based on basilar membraneous length (BML); frequency limits at 60 dB Sound Pressure Level: log(LF)=13(BML-1.2); log(HF) = 391 (BML -0.85). 3. Equation of Hefner & Hefner (2008): log of high-frequency limit = –0.4381 x log (functional interaural delay) + 2.7137); with functional interaural delay (microseconds)= interaural distance/0.3434 (see also Ravel & Orliac, 2015). 4. Equation of Manoussaki et al. (2008) for calculation of low-frequency hearing limit based on the radii ratio (p) of the cochlea: LF = 1.507exp.[−0.578(p-1)].

Table 3a. Dimensions of the semicircular canals of *Ocepeia daouiensis.*

Table 3b. Width (W) and height (H) of the semicircular canals of *Ocepeia daouiensis* (in mm; measurement extending to mid canal section).

Table 3c. Radius of curvature and other measurements of the semicircular canals of *Ocepeia daouiensis*. Radius of curvature calculated following the Spoor–Zonneveld equation (Spoor & Zonneveld, 1998): R= ((H+W)/2/) x 0.5, with H= height and W = width of the canals.

Table 4. Body mass estimates of *Ocepeia daouiensis* (*mean of upper and lower teeth; **estimation = minimal size). Predictive allometric equations from Damuth (1990), Damuth & MacFadden (1990) for all ungulates, selenodonts, and selenodont browsers. The best (i.e., lower) estimates are in bold (mean for all ungulates = 3.5 kg; see text).

Table 5. Plesiomorphic features of *Ocepeia*, with indication of the putative ancestral morphotype taxonomic rank and primary reference inferring character polarity within mammals. References: (1) Billet et al. (2015), (2) Billet et Muizon (2013), (3) Coutier et al. (2018), (4) Ekdale (2013), (5) Ekdale & Rowe (2011), (6) Gheerbrant et al. (2014), (7) Macrini et al. (2007), (8) Macrini et al. (2010), (9) Macrini et al. (2013), (10) Meng & Fox (1995), (11) Muizon et al. (2015), (12) Orliac & O'Leary (2016), (13) Schmitt & Gheerbrant (2016).

Supplementary information

SI 1, Video of the animated 3D CT scan model of the left labyrinth of *Ocepeia daouiensis* from the Paleocene of Morocco, specimen MNHN.F.PM45 (AVI file). Red: fenestra vestibuli; blue: f. cochleae; green: cochleae canaliculus.

SI2, Data for the regression analysis between inner ear height and petrosal size.

SI3, Data added (afrotherians) for the Figure 8, showing the graphical relationships of SCR, BM and agility categories.

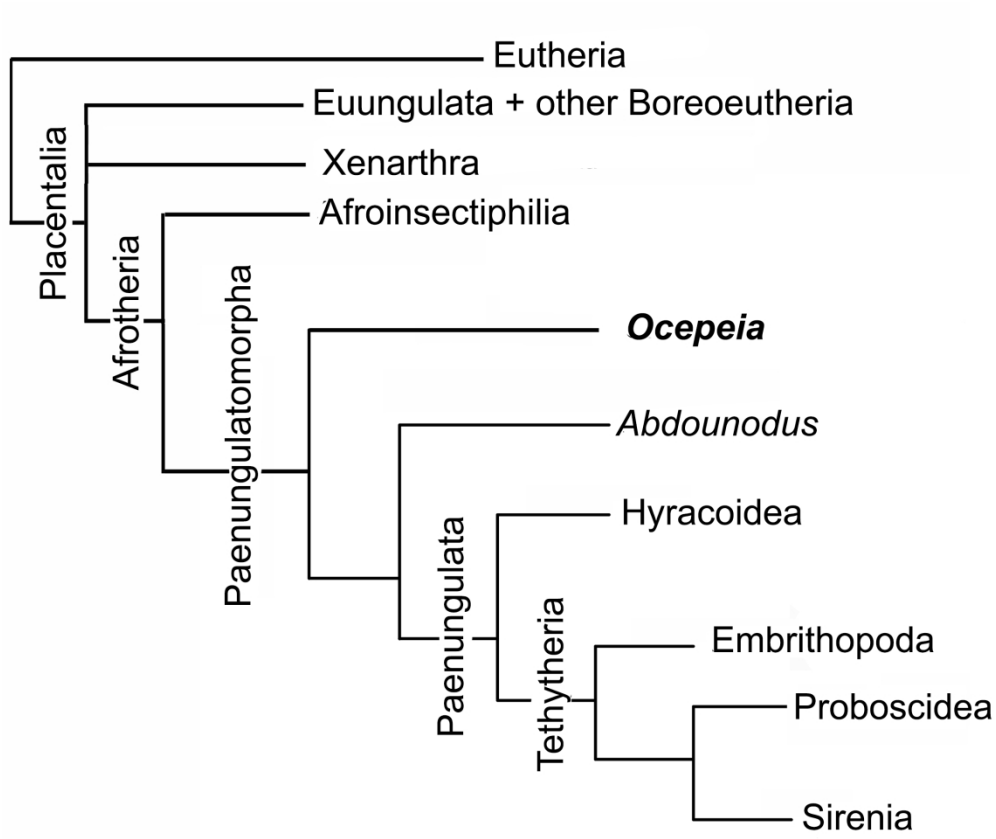

Fig. 1. Simplified cladogram showing the phylogenetic relationships of Ocepeia within Afrotheria (after Gheerbrant et al. 2014, 2016, 2018).

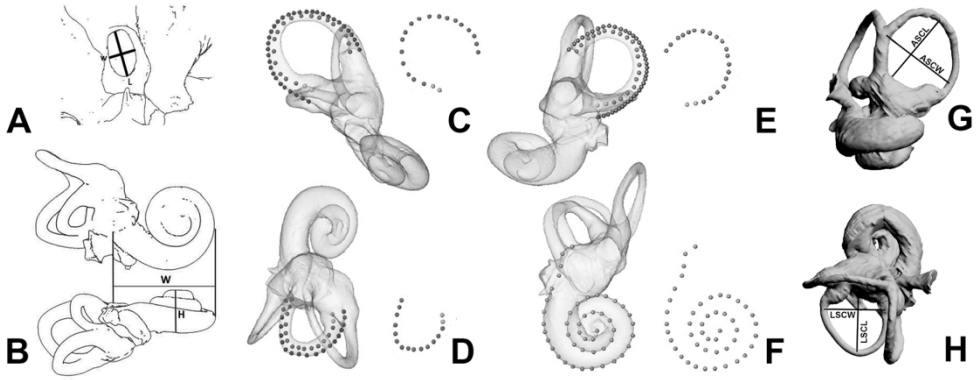

Fig. 2. Measurement protocol of the endocast of the inner ear of Ocepeia daouiensis. (A) stapedial ratio (L = length, W = width); (B) cochlear aspect ratio (H = heigth, W = width): (C) anterior semicircular canal central streamline length, (D) lateral semicircular canal central streamline length; (E) posterior semicircular canal central streamline length: (F) cochlear length; (G) length (ASCL) and width (ASCW) of the anterior semicircular canal used to calculate the radius of curvature; (H) length (LSCL) and width (LSCW) of the lateral semicircular canal used to calculate the radius of curvature.

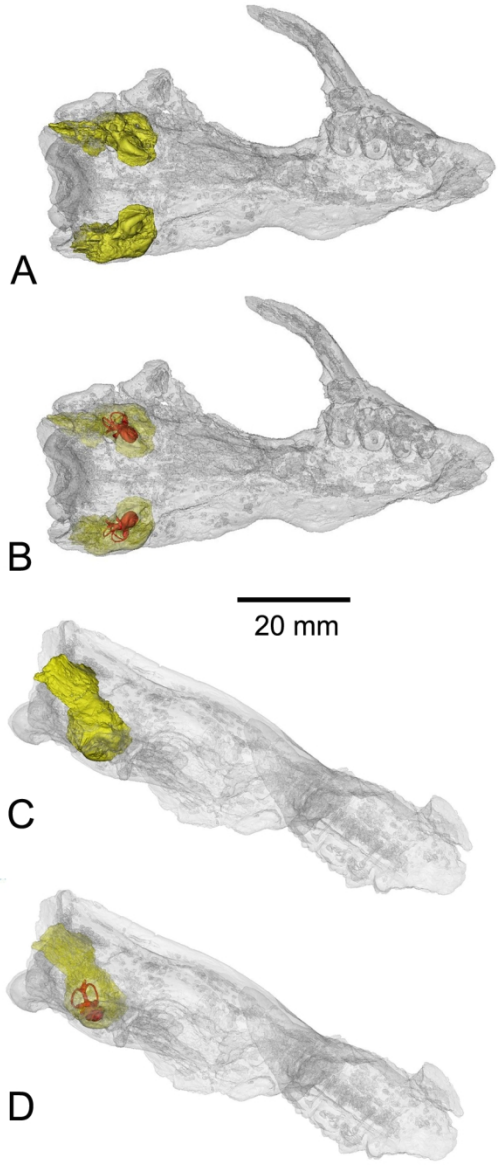

Fig. 3. 3D digital model of the skull MNHN.F.PM45 of Ocepeia daouiensis showing by transparency the petrosal and labyrinth, and the skull posture with the lateral semicircular canal horizontally held (E, F, G). (A-B), ventral views: A, modeling of the petrosals (yellow); B, modeling of the petrosals (transparent, yellow) and labyrinths (red). (C-D), right lateral view with the lateral semicircular canal (SCL) horizontally held: C, modeling of the petrosals (yellow); D, modeling of the petrosals (transparent, yellow) and labyrinths (red). This figure displays the relative small size of the inner ear in the petrosal of Ocepeia daouiensis, the large extent of the mastoid part of the petrosal within the skull and the ventrally inclined posture of the skull in C-D (SCL horizontal).

77x181mm (300 x 300 DPI)

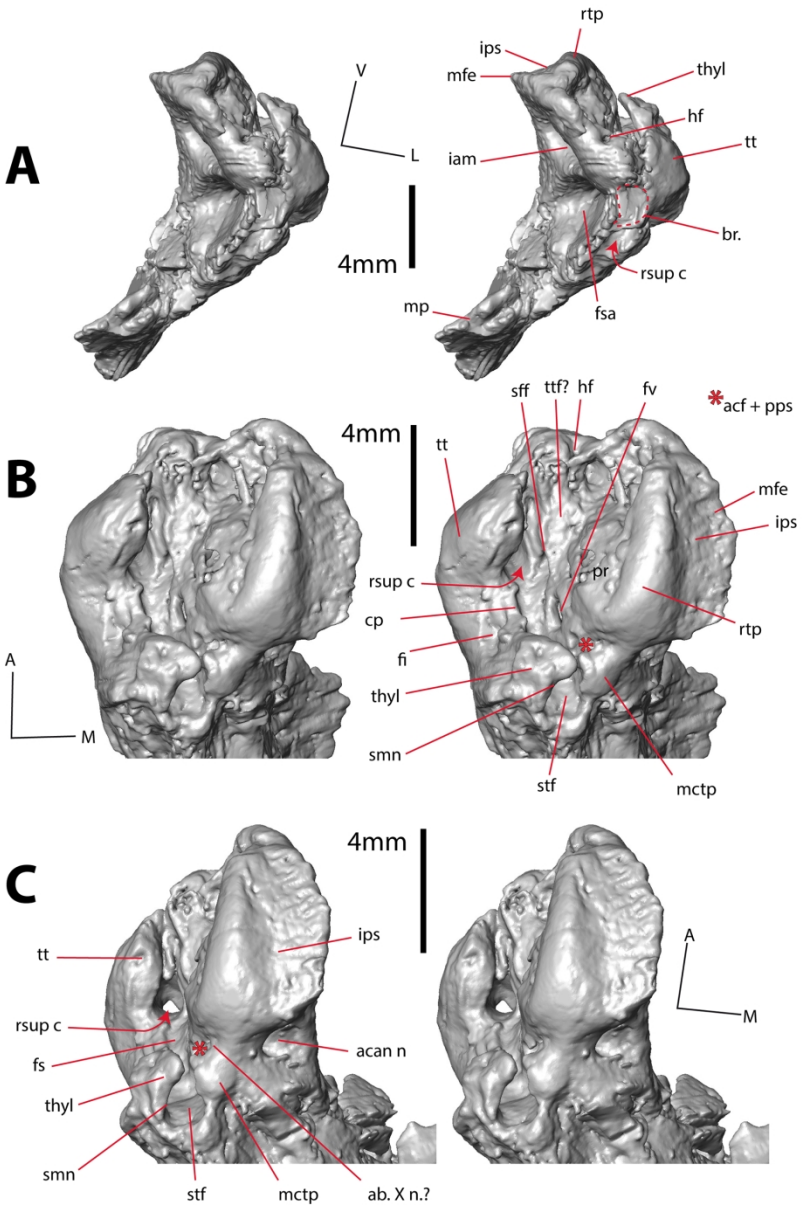

Fig. 4. 3D digital model of the petrosals of Ocepeia daouiensis, skull specimen MNHN.F.PM45. (A), anterior view; (B), ventral view; (C), ventromedial view. Scale-bar: 4mm.
Abbreviations: aav, external aperture of the vestibular aqueduct; ab. X n.?, possible notch/sulcus for the auricular branch of the vagus nerve (X); acan n, notch housing the external aperture of the cochlear canaliculus; acf, external aperture of the cochlear fossula; br., broken area; cp, crista parotica; fai, foramen acusticum inferius; fas, foramen acusticum superius; fi, fossa incudis; fs, facial sulcus; fsa, fossa subarcuata; fv, fenestra vestibuli; hf, hiatus Fallopii; iam, internal auditory meatus; ips, sulcus for the inferior petrosal sinus; mctp, medial caudal tympanic process; mfe, medial flattened edge; mp, mastoid part of the petrosal; pfc, prefacial commissure; pps, postpromontorial tympanic sinus; pts?, possible postemporal sulcus; rsup c, canal for the ramus superior (of the stapedial artery); rtp, rostral tympanic process; sff, secondary facial foramen; smn, stylomastoid notch; ttf, tensor tympani fossa; stf, stapedial fossa; stb?, possible sulcus for temporal branch; stf, stapedial fossa; thyl, tympanohyal; tt, tegmen tympani.

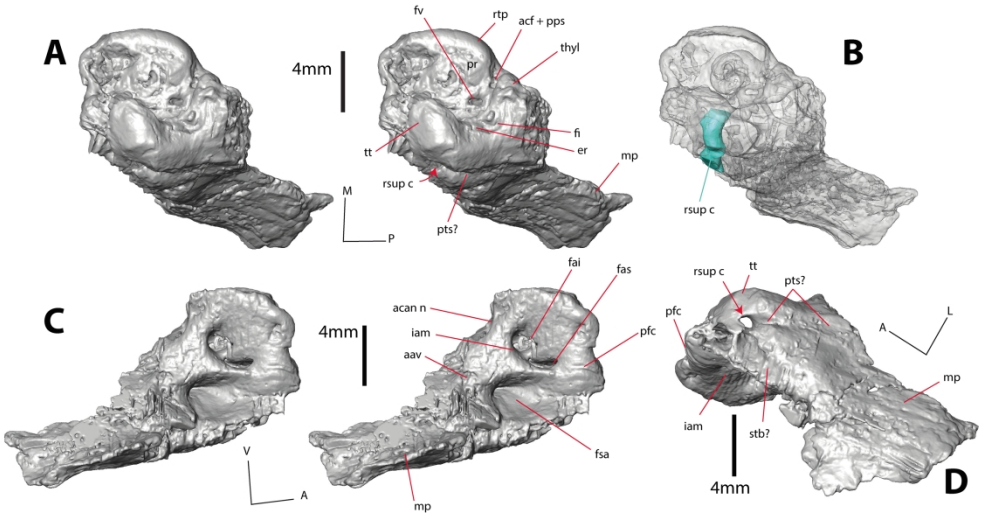

Fig. 5. 3D digital model of the petrosals of Ocepeia daouiensis, skull specimen MNHN.F.PM45. (A), lateral view; (B), lateral view with transparency of the petrosal, and with the canal for the ramus superior of the stapedial artery highlighted; (C), cerebellar view; (D), dorsal view. Scale-bar: 4mm Abbreviations: aav, external aperture of the vestibular aqueduct; ab. X n.?, possible notch/sulcus for the auricular branch of the vagus nerve (X); acan n, notch housing the external aperture of the cochlear canaliculus; acf, external aperture of the cochlear fossula; br., broken area; cp, crista parotica; er, epitympanic recess; fai, foramen acusticum inferius; fas, foramen acusticum superius; fi, fossa incudis; fs, facial sulcus; fsa, fossa subarcuata; fv, fenestra vestibuli; hf, hiatus Fallopii; iam, internal auditory meatus; ips, sulcus for the inferior petrosal sinus; mctp, medial caudal tympanic process; mfe, medial flattened edge; mp, mastoid part of the petrosal; pfc, prefacial commissure; pps, postpromontorial tympanic sinus; pts?, possible postemporal sulcus; rsup c, canal for the ramus superior (of the stapedial artery); rtp, rostral tympanic process; sff, secondary facial foramen; stb?, possible sulcus for temporal branch; stf, stapedial fossa; ttf, tensor tympani fossa; thyl, tympanohyal; tt, tegmen tympani.

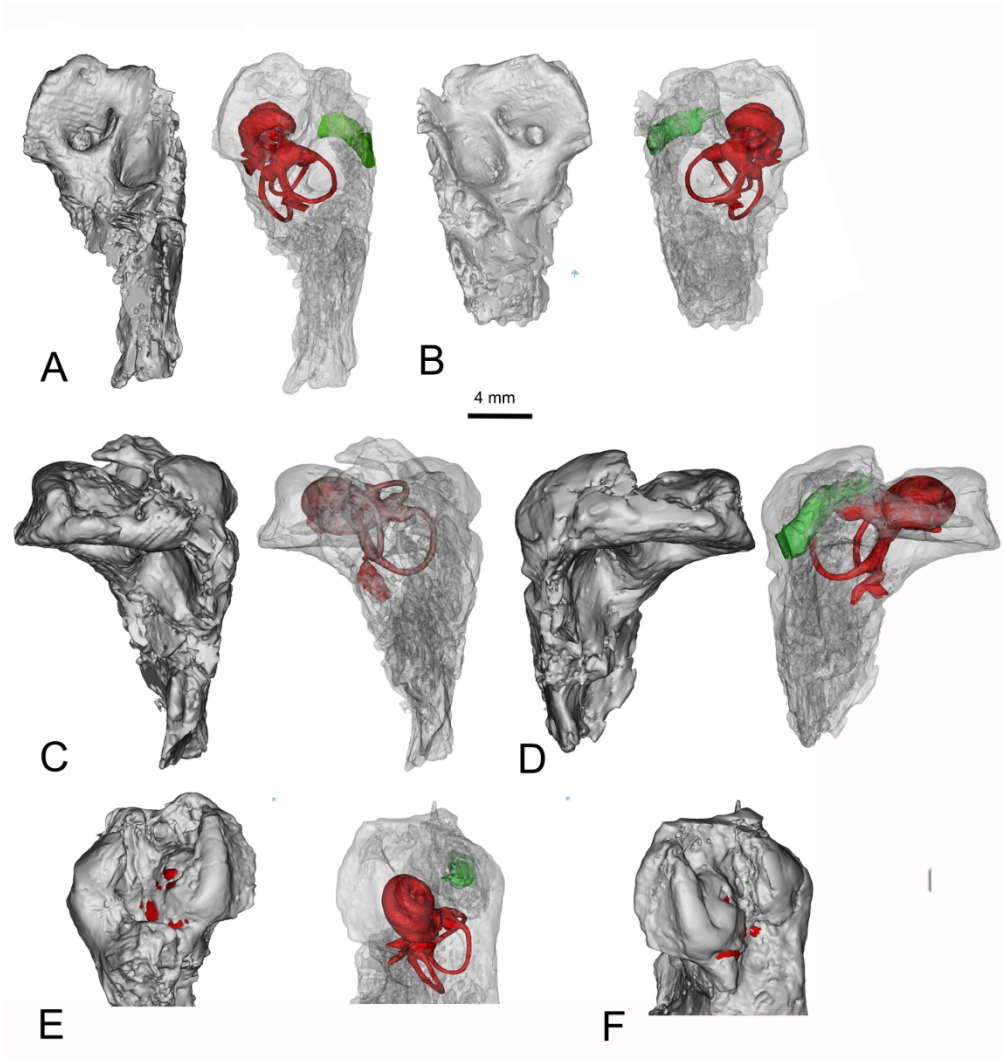

Fig. 6. 3D digital model of the petrosals of Ocepeia daouiensis, specimen MNHN.F.PM45, with the labyrinth by transparency. (A), right petrosal in cerebellar view; (B), left petrosal in cerebellar view; (C), right petrosal in anterior view; (D), left petrosal in anterior view; (E), right petrosal in tympanic view; (F), left petrosal in tympanic view. In red the labyrinth, in green the canal for the ramus superior (of the stapedial artery) within the tegmen tympani. Scale-bar: 4mm

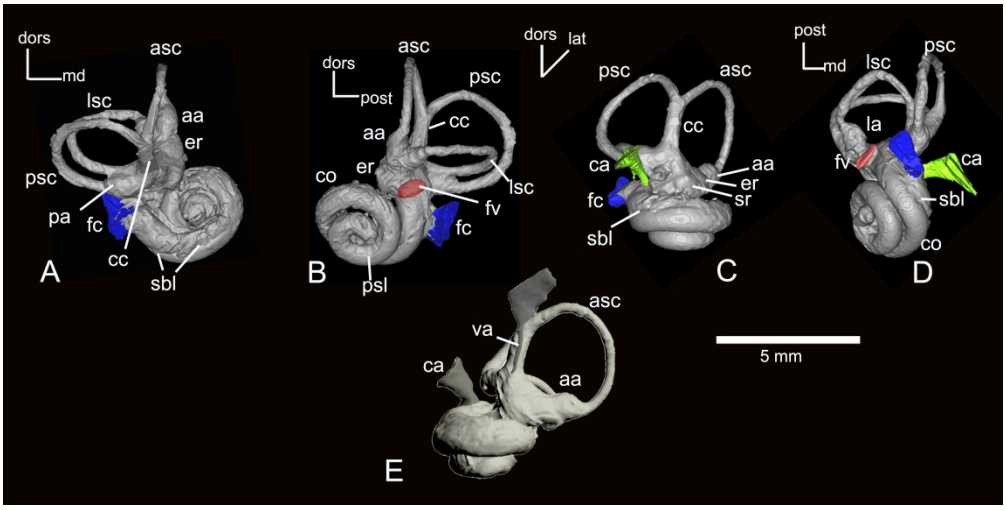

Fig. 7. 3D reconstructed digital model of the left bony labyrinth of Ocepeia daouiensis, specimen MNHN.F.PM45. (A) dorsal view, (B) anterior view, (C) medial view, (D) ventral view and (E) medio-anterior view. Abbreviations: aa anterior ampulla, asc anterior semicircular canal, av aquaeductus vestibuli, cc crus commune, cca cochlear canaliculus, co cochlea, er elliptical recess, fc fenestra cochleae, fv fenestra vestibuli, la lateral ampulla, lsc lateral semicircular canal, pa posterior ampulla, psc posterior semicircular canal, sbl, secondary bony lamina, sr, spherical recess, va, vestibular aqueduct. Orientation axes: dors dorsal; md medial, lat lateral, post posterior.

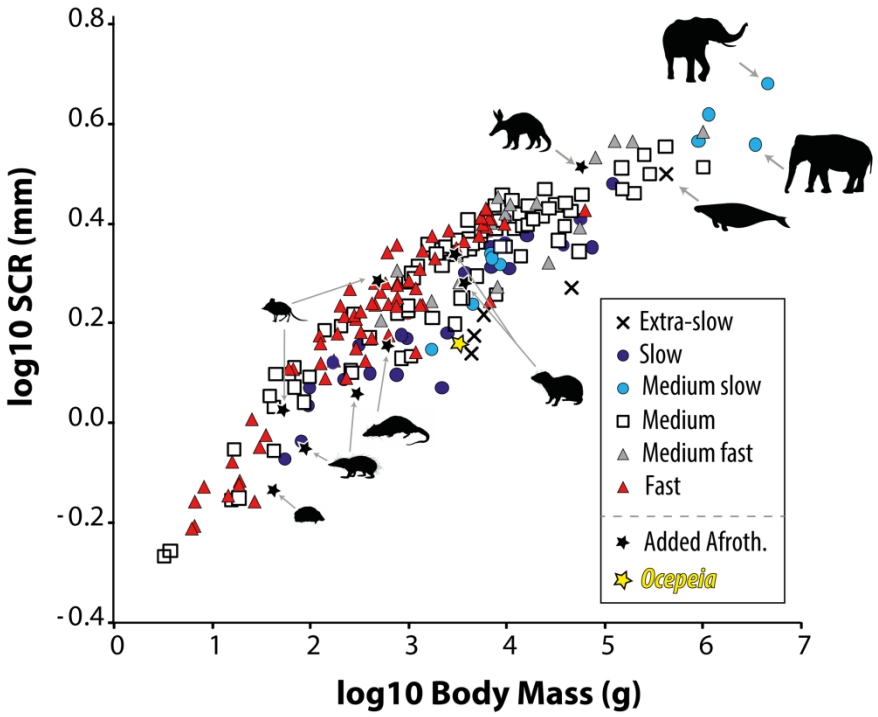

Fig. 8. Graphical relationship between the size of the semicircular canals (SCR, radius of curvature) versus body-mass (BM), with the indication of agility estimates in various mammals as measured and compiled by Spoor et al. (2007). Measurements for Ocepeia daouiensis, and several extant afrotherians such Orycteropus, Macroscelides, Rhynchocyon, Procavia, Dendrohyrax, Potamogale, Tenrec, Tenrec, Chrysochloris, Hemicentetes were added to the dataset (silhouettes from PhyloPic website) (see SuppData S3). This diagram shows that Ocepeia and the insectivore-like afrotherians (Tenrecoidea) are characterized by a relative small size of the semicircular canals with respect to other mammals of the same body mass.

Measurements and Ratios (mm)	*Mimoperadectes houdei* USNM 482355	morphotype VIII Itaborai Metatheria MNRJ 6735-V (with PET H estimated from other specimens)	morphotype euth. I Tiupampa MHNC uncatalogued	morphotype euth. II Tiupampa MHNC uncatalogued
PET L	4.41	1.34	7.23	5.08
PET W	6.23	1.43	5.93	4.40
PET H	6.66	2.67	9.67	6.65
(PET L + W + H) /3 = PET size	5.77	1.81	7.61	5.38
IEH	4.23	2.32	5.15	3.51
log PET size	0.76	0.26	0.88	0.73
log IEH	0.63	0.37	0.71	0.55
	Billet et al 2015	Billet et al 2015	Billet et al 2015	Billet et al 2015

Ocepeia	
log IEH	0.755
log PIMS	0.987

Tamandua tetradactyla UMCZ E581	*Choloepus didactylus* UMCZ E81	*Megatherium* sp. MNHN-F-TAR 1291	*Alcidorbignya inopinata* MHNC 8360	*Baioconodon nordicum* YPM-PU 14234	*Didelphodus altidens* USNM 18369
8.11	10.71	51.50	5.25	5.55	5.22
11.89	11.15	45.10	5.96	5.67	4.64
14.76	13.51	54.40	7.80	7.98	6.29
11.59	11.79	50.33	6.34	6.40	5.38
9.06	8.52	20.37	4.33	4.71	3.77
1.06	1.07	1.70	0.80	0.81	0.73
0.96	0.93	1.31	0.64	0.67	0.58
Billet et al 2015	Billet et al 2015	Billet et al 2015	Billet et al 2015	Billet et al 2015	Billet et al 2015

Deltatherium sp. AMNH 16610	*Procavia capensis* STIPB M6605	*Astrapotherium* sp. MNHN-F-SCZ 8	Notoungulata MNHN-F-BRD 23	Notoungulata UFRJ-DG 1039M	Elephantimorph 1 TMM 933-950
9.10	9.93	20.84	7.03	8.51	40.00
9.20	7.98	23.19	6.16	8.95	51.25
11.72	9.94	42.71	7.31	9.81	56.25
10.01	9.28	28.91	6.83	9.09	49.17
5.67	8.08	13.27	5.26	6.15	19.00
1.00	0.97	1.46	0.83	0.96	1.69
0.75	0.91	1.12	0.72	0.79	1.28
Billet et al 2015	Billet et al 2015	Billet et al 2015	Billet et al 2015	Billet et al 2015	Billet et al 2015

Leptictis sp. AMNH 80213	*Mus musculus* STIPB M1082	*Sciurus vulgaris* STIPB M887	*Myocastor coypus* GB coll.	*Erinaceus europaeus* STIPB M174	*Sorex cinereus* STIPB M119
6.51	3.62	7.99	10.90	5.57	2.17
7.21	4.01	5.26	12.50	6.25	2.38
8.67	4.16	10.61	17.20	9.54	3.62
7.46	3.93	7.95	13.53	7.12	2.72
5.33	3.67	6.38	9.45	5.71	3.07
0.87	0.59	0.90	1.13	0.85	0.44
0.73	0.56	0.80	0.98	0.76	0.49
Billet et al 2015	Billet et al 2015	Billet et al 2015	Billet et al 2015	Billet et al 2015	Billet et al 2015

Martes sp. GB coll.	*Felis chaus* ZFMK 2008.214	*Panthera tigris sumatrae* ZFMK 86.118	*Pipistrellus pipistrellus* ZFMK 2014.461	*Coelodonta antiquitatis* STIPB M1655	*Diceros bicornis* MNHN-ZM-AC 1996.2520
8.99	13.25	25.21	2.26	22.40	30.76
6.69	9.72	17.94	1.62	30.07	16.00
7.79	13.10	19.36	2.25	31.58	37.50
7.82	12.02	20.84	2.04	28.02	28.09
6.48	8.74	13.60	2.43	14.61	13.49
0.89	1.08	1.32	0.31	1.45	1.45
0.81	0.94	1.13	0.39	1.16	1.13
Billet et al 2015	Billet et al 2015	Billet et al 2015	Billet et al 2015	Billet et al 2015	Billet et al 2015

Miguelsoria UFRJ-DG 1036M	*Miguelsoria* UFRJ-DG 1035M	*Miguelsoria* UFRJ-DG 119M	*Miguelsoria* UFRJ-DG 347M	*Miguelsoria* UFRJ-DG 275M	*Macrauchenia patachonica* MNHN-F-PAM 69
6.84	7.15	6.81	7.51	7.61	25.97
7.18	6.18	6.72	7.89	6.86	21.01
9.68	8.36	8.63	9.31	9.18	38.29
7.90	7.23	7.39	8.24	7.88	28.42
5.62	5.61	5.64	6.63	5.69	15.66
0.90	0.86	0.87	0.92	0.90	1.45
0.75	0.75	0.75	0.82	0.76	1.19
Billet et al 2015	Billet et al 2015	Billet et al 2015	Billet et al 2015	Billet et al 2015	Billet et al 2015

Diadiaphorus sp. MNHN-F-SCZ 3	*Proterotherium* sp. MNHN-F-SCZ 205	*Pleuraspidotherium aumonieri* MNHN-F-BR uncatalogued	Panameriungulate? GROUP 1 UFRJ-DG 127M	Panameriungulate? GROUP 1 UFRJ-DG 1044M	Panameriungulate? GROUP 1 UFRJ-DG 354M
19.57	15.86	10.81	16.28	13.96	11.79
11.55	9.99	10.42	12.45	-	11.46
24.68	17.76	14.51	17.02	-	17.82
18.60	14.54	11.91	15.25	13.96	13.69
11.05	9.55	6.09	7.32	7.81	7.31
1.27	1.16	1.08	1.18	1.14	1.14
1.04	0.98	0.78	0.86	0.89	0.86
Billet et al 2015	Billet et al 2015	Billet et al 2015	Billet et al 2015	Billet et al 2015	Billet et al 2015

Panameriungulate? GROUP 2 UFRJ-DG 124M	Panameriungulate? GROUP 2 UFRJ-DG 1046M	Panameriungulate? GROUP 3 UFRJ-DG 1045M	Panameriungulate? GROUP 3 UFRJ-DG 125M	Panameriungulate? GROUP 4 RHcoll uncatalogued		Ocepeia
9.73	8.67	12.49	14.95	8.22		8.91
10.22	6.39	10.03	12.42	9.07		6.29
14.73	10.73	15.50	15.49	10.72		10.13
11.56	8.60	12.67	14.29	9.34		8.44
6.44	5.62	7.09	6.37	6.06		5.65
1.06	0.93	1.10	1.15	0.97		0.93
0.81	0.75	0.85	0.80	0.78		0.75
Billet et al 2015	Billet et al 2015	Billet et al 2015	Billet et al 2015	Billet et al 2015		

Phosphatherium	Eritherium
11.88	5.53
9.88	6.89
10.91	8.92
10.89	7.11
7	5
1.04	0.85
0.85	0.70

IEH estimated for *Eritherium* and *Phosphatherium* (petrosal damaged

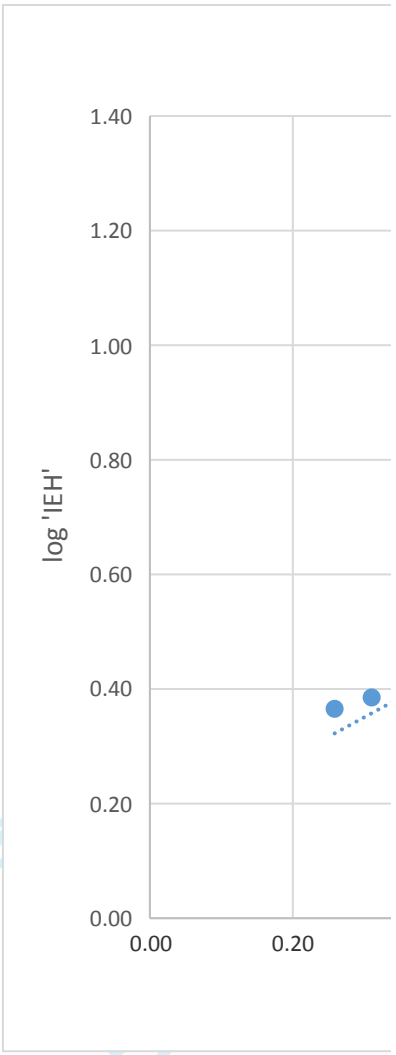

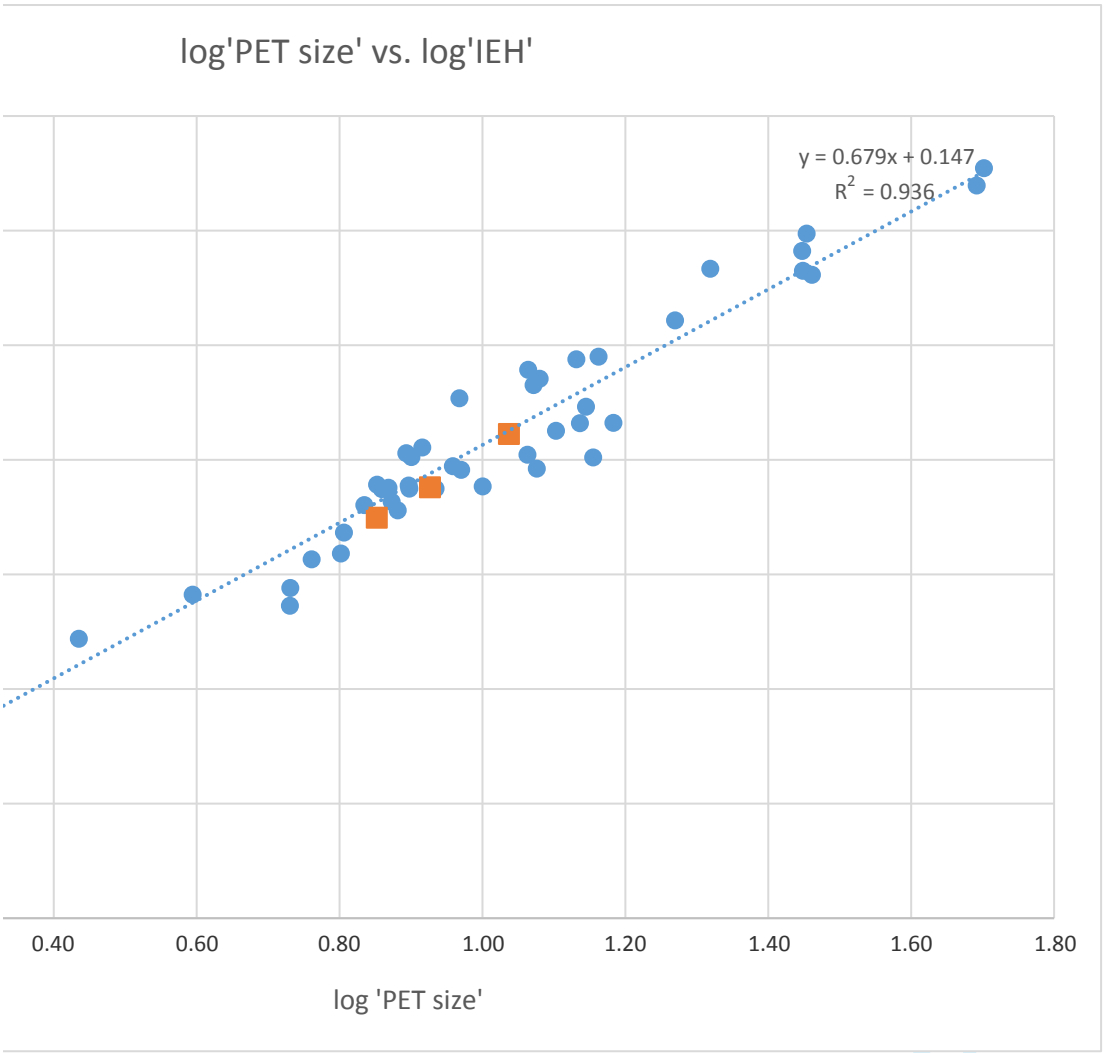
log'PET size' vs. log'IEH'
y = 0.679x + 0.147
R2 = 0.936
0.40
0.60
0.80
1.00
1.20
1.40
1.60
1.80
log 'PET size'

Data Set 1. Species mean values used in analyses of semicircular canal dimensions								
Taxon	**Order**	**Family**	**BM, g**	**ASCR, mm**	**PSCR, mm**	**LSCR, mm**	**SCR, mm**	**logBM**
Ocepeia			3500				1.42	3.544
Macroscelides								1.732
Rhynchocyon								2.690
Procavia			3800	2.12	1.66	1.97	1.92	3.580
Dendrohyrax			3000	2.30	1.97	2.38	2.22	3.477
Orycteropus afer SMF 15605			60000	3.53	3.04	3.31	3.29	4.778
Potamogale velox MNHN 1898-1576			600	1.56	1.30	1.41	1.42	2.778
Tenrec ecaudatus UMZCTenrec6			300	1.29	1.01	1.14	1.15	2.477
Chrysochloris SMF26853			42	0.920	0.660	0.620	0.73	1.623
Hemicentetes semispinosum (in Ekdale 2013)			90	1.100	0.680	0.890	0.89	1.954
BM, body mass; ASCR, anterior semicircular canal radius; PSCR, posterior semicircular canal radius; LSCR, lateral semicircular canal radius; SCR, average semicircular radius.								

logAGILITY	logASCR	logPSCR	logLSCR	logSCR			
				0.152			this study
				0.025			Ruf et al 2016
				0.289			Ruf et al 2016
				0.283			Benoit et al 2016 + BM from Walker's M
				0.346			Benoit et al 2016 + BM from Walker's M
				0.518			Benoit et al 2016 + BM from Walker's M
				0.153			Benoit et al 2015 + BM from Handbook
				0.059			Benoit et al 2015 + BM from Handbook
				-0.135			Benoit et al 2015 + BM from Handbook
				-0.051			Ekdale et al 2013 + BM from Handbook

lammal of the World
lammal of the World
lammal of the World
Mammals of the World
Mammals of the World
Mammals of the World (same as C stuhlmanni)
Mammals of the World